FACULTY OF SCIENCE
UNIVERSITY OF COPENHAGEN

Master's thesis

Shahid Aftab Mir

Physical changes of nucleic acids induced by fullerenes

A single molecule study

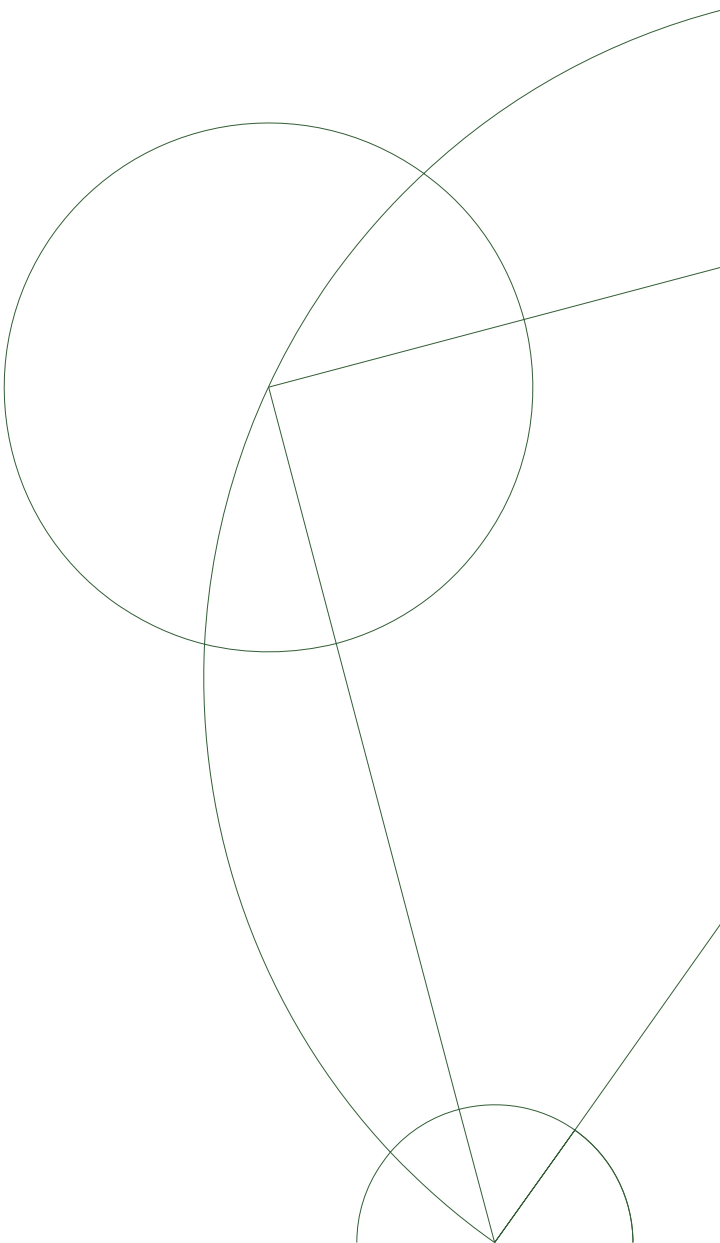

Academic advisor: Lene B. Oddershede

Submitted: 01/03/10

Preface

This Ms.C. thesis was performed in the Optical Tweezers group at the Niels Bohr Institute in Denmark.

I would like to express my greatest appreciation to a number of people, who have played a special role for the results obtained in the project.

My deepest gratitude goes to my supervisor Lene Oddershede for taking me as her Ms.C. student to work on this highly interesting topic. Special thanks goes to Fabian Czerwinski for guiding me trough the work in the lab, especially problem solving and spending lots of hours on discussions.

I would also like to thank the Optical Tweezers group with Nader who I spent a lot of time with in the lab and who was kind to share his knowledge, Anders Rosengren for his proof-reading and Andrew and Tabita for their kind spirits.

Last but not least I would like to thank my family for their support.

Abstract

The topic of this project is C_{60} fullerenes interaction with DNA. To study this interaction, DNA is tethered between two beads, by means of an optical trap. By pulling on one of the beads with the trap, it is possible to measure an elastic force response from the DNA in the picoNewton range. Mathematical models can be used to characterize this response by a persistence length which explains the DNA's stiffness. By comparing the persistence length before and after the addition of C_{60} to DNA, it is possible to measure this response.

Results from this thesis will show that DNA does have a different stiffness due to exposing to C_{60}. This implies that C_{60} does attach to DNA which is detrimental.

Table of Contents

1 Introduction

Recently remarkable and seemingly innovative products containing nanoparticles have been launched for private consumers, among others; transparent sun blocking cream and anti-bacterial soap. One could worry that this new sensational technology might have hazardous effects. Like asbestos which previously was widely used and now know to cause cancer. Genotoxicity by exposure to C_{60} fullerenes, a spherical carbon structure, in water has been reported (1). These include experiments on live rats exposed to C_{60} where a genotoxic affect (2), related to cancer by oxidatively damaging nuclei-acids, have been found.

By using optical trapping it is possible to perform experiments on a single DNA, probing its elastic response to forces in the pico-newton range. The method has been employed in this thesis by optically trapping a bead which has been incubated with DNA. Moving the trap near another, specifically coated, bead one end of the DNA can tether to it by bonding specifically. Extending the DNA a force-extension relationship can be measured. Data from the measurements can be fitted to theoretical models for DNA, whereby a persistence length can be obtained describing the stiffness of the molecule.

The goal of this thesis is to measure any conformal changes in DNA induced by C_{60}. Experiments are preformed inside custom built microfluidic chambers which are connected to a precision pump. This allows a constant flow of C_{60} to enter the chamber. By first acquiring force extension curves in the absence then the presence of C_{60}, the DNA conformational change due to its stiffening can be deducted through the persistence length.

The thesis can be divided up into several sections. The first section will elaborate on what optical tweezers are and how they work, alongside with experiments performed to test the microfluidic chambers and the pump. Further experiments are done to improve the trapping strength.

The next section explains how DNA tethers are formed, where after the C_{60} molecule, including presentation of observations, is described. The last section is regarding force-extension curves, the process of acquiring those and presentation of the data.

2 Trapping of colloidal particles by light

An explanation of the forces imparted on a bead from a laser is followed. Thereafter a bead's movement in the presence of laminar flow is described. The trap-calibration method used in this report is presented at the end of this chapter, with the main highlights summarized.

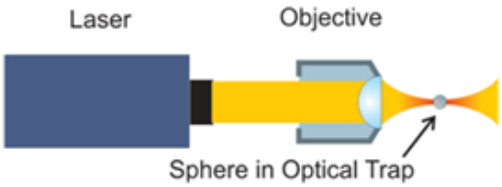

Figure 1: Measurement principles: Trapping a bead with a laser, where the bead is surrounded by fluid having a flow. (4)

2.1 Focus of laser

'Optical tweezers' (OT) are in essence a laser beam sent through an objective whereby it is focused see Figure 1. When the beam is focused on a desired object, forces interact between the object and laser.

Thus by the use of OT, it is possible to manipulate (3)objects in the microscopic scale e.g. DNA (4), proteins (5)or an array of molecules (6). In some instances polystyrene spherical beads are used to facilitate experiments with optical tweezers.

The lasers wavelength λ is 1064 nm, since using light in the infrared region will have a minimal damage on biological entities. Experiments were done with two beads with diameters *d* of 1.48µm and 3.04µm, so d~ λ.

The laser has a TEM_{00} mode with a Gaussian intensity profile. The intensity of a Gaussian beam can be written as: $I \sim e^{-x^2 y^2}$. The laser has a very large beam waist compared to the bead. To achieve a smaller waist the beam is sent through an objective where it gets refracted, and converges to a diffraction limited spot. It is this central spot of high intensity, which is the source of the forces that keeps a bead in a trap.

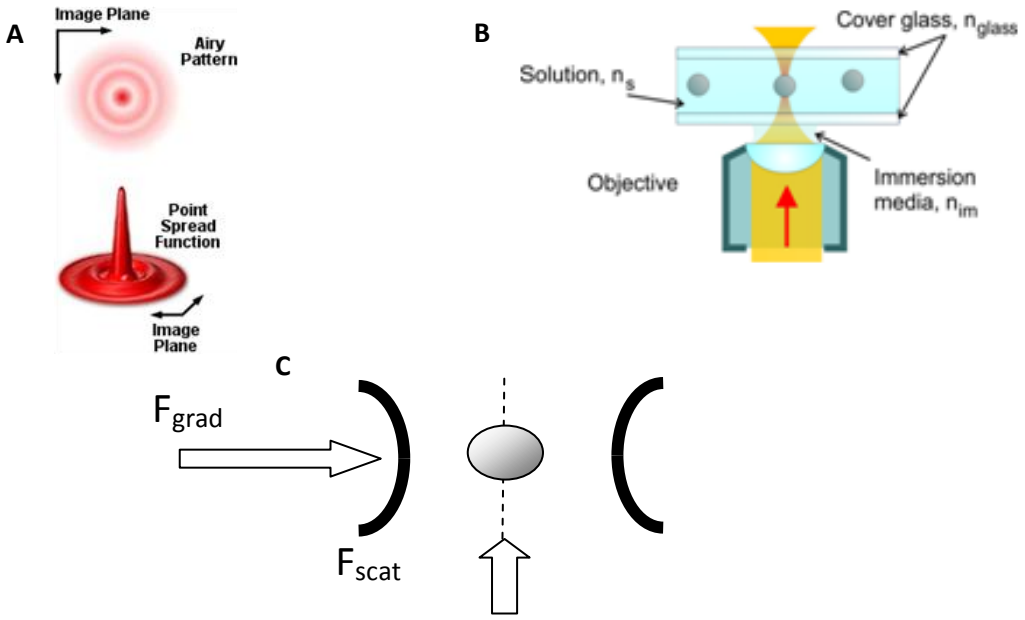

Figure 2: A). When the beam gets refracted through the objective it does not converge towards a point, rather an Airy pattern is formed, caused by diffraction. Figure A) shows disks with a darker spot in the center. The cone shaped figure is the point spread function (PSF) which is a 3-D representation of the same disks. Intensity is highest at the center (15). B). That the objective is plan apochromatic refers to corrected aberrations including spherical aberration. Magnification: 63x, Numerical Aperture: 1.20, and should be used with water as the immersion medium (4). C). With higher laser intensity the bead is 'pulled' in faster towards the center of the trap. One can imagine that higher intensity also increases the scattering force. High intensity gives a stronger trap, and a higher/steeper PSF profile.

Figure 2 B): Circular resembling diffraction patterns created by this spot can be seen at different interfaces. The objective is used with water and the condenser with oil. Using a water objective gives the possibility to focus throughout the chamber.

Figure 2 C): In practice when using OT two types of forces are experienced by the beads. If the focus is positioned below the bead, closer to the objective, immediately the bead will get out of view. It is usually found above the previous focused position. On the other hand when bead is below the focus it will get pushed up into the trap. Thus at least an axial force works on the bead. Another force works more like a magnet or a spring mainly in the lateral direction but also in the axial. When moving the focus near a bead and if the proximity is close enough, the bead begins to approach the laser beam. First moving slowly and then increasing its velocity until it ends up inside the trap. This is called the gradient force.

If the bead has $d > \lambda$ the interaction between the laser and the bead can be explained as follows. The laser is seen hitting the bead with individual rays, and as known from Snell's formula these rays will get refracted, the degree of which depends upon the

relative index of refraction. In case of the experiments performed: *n (water) <n (bead)*, the rays will tend towards the surface normal of the bead. Each ray being a photon will have a momentum, which changes upon refraction, since its direction changes. Since there are no other forces to act on the bead (7), conservation of momentum results in the bead getting a momentum equal to that of the change in the rays. Because of the Gaussian profile, a higher intensity near the optical axis, translates into more photons. Having a strong momentum in the optical axis, means that when whenever the bead is displaced transversely or laterally, it returns to what can be called equilibrium. Equilibrium would be the laser focus, where all the rays are refracted symmetrically along the optical axis. The bead is displaced slightly from this point of equilibrium due to scattering, scattering force works in the direction of the propagating rays, hence the shift in equilibrium (7), (8).

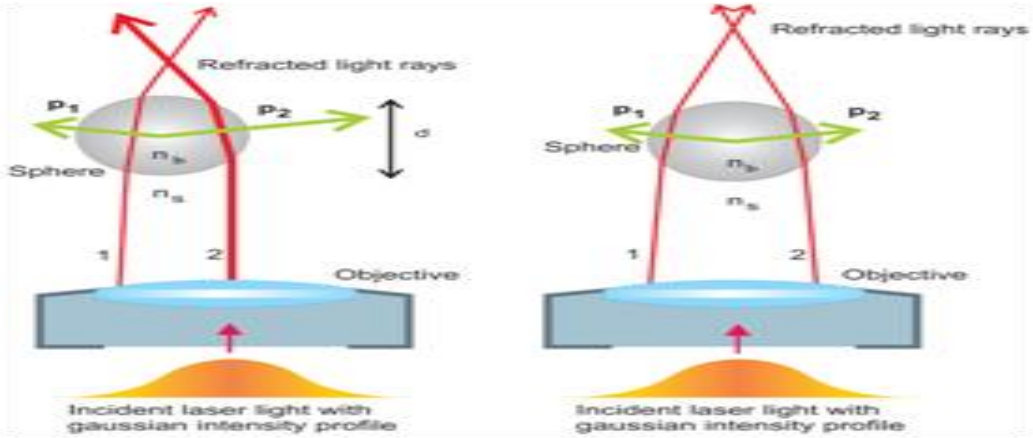

Figure 3 Illustrating laser light with Gaussian intensity profile propagating through a lens and afterwards a bead, when $n_b > n_s$ and $d > \lambda$. Left side shows a bead which is dislocated to the left with respect to the optical axis. Individual rays with their associated impulses are impinging on the bead. Ray 1 is thin because the laser intensity is low, it gets refracted to the right which gives the bead same amount of momentum change P1 to the left. Rays emanating at the optical axe impart more momentum P2 on the bead, thus total impulse forces the bead to align with the objective. The right side of the image depicts the bead now in equilibrium in the horizontal level, but impulses will exert a force on the bead towards the converging beam. (4)

2.2 Motion of free and trapped colloids

The gradient force can be explained in analogy to a spring, and higher laser intensity results in more momentum transfer to a trapped bead. Thus a strong trap is correlated to a high trap stiffness through the spring constant.

This section is divided up in two subsections. First the random walk of a sphere and the restriction imposed on it by a laser trap will be explained. It will then be possible to connect a beads movement to the spring constant. An elaboration on the shear forces in a flowing fluid and the resulting velocity is given in the second section.

2.2.1 Diffusion of colloids in solution

Consider a bead in an aqueous solution, which is isolated so no external forces are prevalent and the system is in its canonical state. The bead is observed through a microscope, one notices that it is making a 'jittering' movement, called Brownian motion which is random and attributed to diffusion. The surrounding water molecules have kinetic energy, by transferring momentum to the beads results in the observed jittering. The stochastic force imparted on the bead from the surrounding molecules is denoted by *F (t)*. When the bead gains a velocity it will be subjected to a drag force. The force to drag a sphere in a fluid is given by stokes' law $F = -\zeta v$, $\zeta = 3\pi\eta d$ is the drag coefficient (9), η viscosity, d diameter, where *v* is the velocity of the bead with respect to the water.

The equation of motion the bead in the microscopic scale is called the Langevian equation (9):

$$m\ddot{x} = F(t) - \zeta\dot{x} \ . \tag{1.1}$$

By solving the above equation for the square root mean displacement for long time scale and $\langle F(t)\rangle = 0$, gives $\langle x^2\rangle = 2Dt$ in two dimensions, with $D = \frac{k_B T}{3\pi\eta d}$ (9) being the diffusion constant for a sphere, and η viscosity of the solution.

A dielectric bead will 'feel' a force generated from the laser, depending on the gradient of the laser beams intensity profile. A bead in an optical trap will feel a harmonic potential (10) from a laser beam with a Gaussian profile, in 1 dimension:

$$U(x) = \frac{1}{2}k\langle x^2\rangle \ . \tag{1.2}$$

Then the force can be interpreted as harmonic oscillator: $F = -kx$. The harmonic potential describes the bead as being confined to a volume and the force retaining it would be proportional to its displacement from equilibrium, here *k* is the stiffness of the laser trap and can be seen as a spring constant.

Equipartition theorem states that each degree of freedom (of the molecules) has an energy average of $\frac{1}{2}k_bT$ and in a potential as the one described above, the bead will have exactly one degree of freedom.

The situation is thus far that the bead is getting energy from the molecules and it 'sees' itself in a harmonic potential trap:

$$\frac{1}{2}k\langle x^2\rangle = \frac{1}{2}k_bT \rightarrow k = k_b\frac{T}{< x^2 >} . \quad (1.3)$$

2.2.2 Parabolic shear stress

When a trapped bead is subjected to a flow, a velocity *v* dependent drag force is imparted on in. Experiments are performed by trapping a bead at different heights inside a flow chamber during a constant flow, to investigate the parabolic velocity flow profile. This section will describe dependency of *v* on the distance from the surface. The flow is created by a precision pump see Figure 12.

With Navier-Stokes equations it is possible to express relationships concerning fluid dynamics, in this case describing a fluids equation of motion (11):

$$\rho\left(\frac{\partial \mathbf{v}}{\partial t} + \mathbf{v}\cdot\nabla\mathbf{v}\right) = -\nabla p + \eta\nabla^2\mathbf{v} , \quad (1.4)$$

ρ being the fluid density, *v* the flow velocity, p the pressure and μ the viscosity constant. Left side has an acceleration term $\frac{\partial \mathbf{v}}{\partial t}$, and a term for the fluids convection with respects to space. Both of these terms times ρ gives the inertial term. Right side relates to the gradient of pressure ∇p, and the viscosity. With static fluid $\nabla p = 0$ and no forces are created.

A dimensionless number which describes fluids is the Reynolds number (12) (9) , which is a ratio of: density ρ, velocity *v*, viscosity μ, and the length scale L which is the height of the chamber where velocity changes. The Reynolds number describes the ratio between inertial and viscous forces and is expressed by:

$$Re \equiv \frac{\rho v L}{\eta} .$$

It is valid for both fluids and objects immersed in fluids. For Re<1 viscous forces will dominate and laminar flow is present (4).

With Re < 1[Appendix A], inertial forces are suppressed then there should not be any acceleration, i.e. a smooth flow without swivels and vortexes. The left side inertial term of eq. (1.4) vanishes leaving (11):

$$\nabla p = \eta \nabla^2 \boldsymbol{v} \ . \qquad (1.5)$$

Timing both sides with area results in two forces: $A'\nabla p = A''\eta\nabla^2 v$, A' is a cross section area where the pressure difference exists. A'' is the area associated with the viscosity.

Laminar flow can be characterized by dividing the fluid into layers, where each layer has different velocity e.g. higher from the wall of the chamber to the center. In Figure 4 a blue layer is dragged though water with a constant velocity it will transfer some of its momentum to the lower layers.

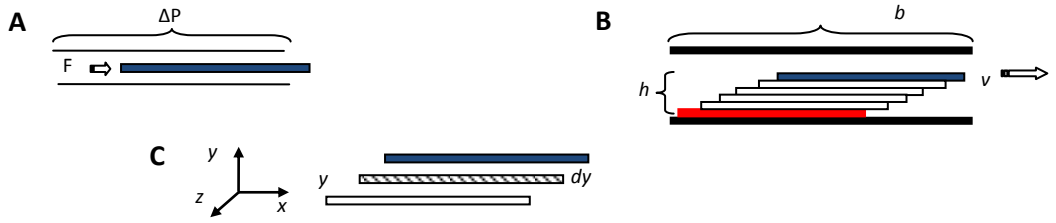

Figure 4 A) B) C) Illustrating different fluid layers.

The force created by the pump is: $F_{pump} = P \cdot A = \Delta P w dy$, ΔP pressure gradient, w being the width of the chamber and w>>h so to discard any effects from the side walls. Since the layers have different velocities this creates shear (resistance), and the force to move the layers is called viscous force $F = -\eta A \frac{\partial v}{\partial y} = -\tau A$ (12)where A is the area of one plate and v is the velocity of the layer, note same term from eq. (1.5). The relative velocity between layers is linear $v(y) = \frac{v(h)y}{h}$ (12)the second derivate with respect to y is shear. A general condition applies when dealing with flow at boundaries. A fluids velocity decreases when it is nearer to the walls to a point where the no-slip boundary condition applies, which in practice means the flows velocity in Figure 4 B (red) is zero, at the walls of the chamber. By equating the net shear on a layer (Figure 4 C grey) and equating that to F_{pump} gives an expression for the velocity inside the chamber. In Figure 4 C), the net viscous force on one layer (gray) arises from the fluid interaction on the layers bottom and top part (12):

$$F_{net,viscous} = \eta b w \left[\left(\frac{\partial v_x}{\partial y} \right)_y - \left(\frac{\partial v_x}{\partial y} \right)_{y+dy} \right] = \eta b w \left[\left(\frac{\partial v_x}{\partial y} \right)_y - \left(\left(\frac{\partial v_x}{\partial y} \right)_y + \left(\frac{\partial^2 v_x}{\partial y^2} \right) dy \right) \right]$$

$$\underset{dy \to 0}{=} -\eta bw\left(\frac{\partial^2 v_x}{\partial y^2}\right)dy$$

In the bracket the first part is of the bottom section which feels a drag from slower moving layers, the derivative is negative. Second parentheses represents the top part, since the curvature is negative it force is "pulling" the layer. Equating: $F_{pump} = F_{viscous}$ gives (12):

$$\frac{d^2v}{dy^2} = -\frac{\Delta P}{\eta b}$$

To find the velocity profile integrating the equation above is required:

$$\iint d^2v = \frac{\Delta P}{\eta b}\iint -1 \cdot d^2y \to -\int dv = \int \frac{\Delta P}{\eta b}(-y + c_1)dy$$

$$=> v(y) = \frac{\Delta P}{\eta b}\left(-\frac{1}{2}y^2 + yc_1 + c_2\right),$$

Using the no-slip boundary conditions: $v(0) = v(h) = 0$, gives $c_2 = 0, c_1 = \frac{1}{2}h$ resulting in (12):

$$v(y) = \frac{1}{2}\frac{\Delta p}{\eta b}y(h - y)\ . \qquad (1.6)$$

The velocity is dependent on the distance to the walls. Maximum velocity is achieved at the center between two walls when y = h½, and least velocity near the walls. The overall profile is that of a parabolic. Subsequently trapping a bead, during a constant flow, in the center of chamber should subject it to the highest drag force. The least amount of drag on the bead should be near the edges of the chamber. Experiments will infer that the drag force has a parabolic form in between the walls of the chamber.

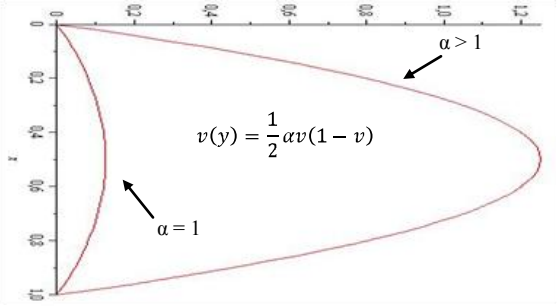

Figure 5 shows a diagram where the vertical axis is the normalized height of the rectangular chamber from [0:1] and the horizontal axis represents the velocity. The diagram is illustrating the parabolic velocity profile inside a rectangular chamber. A normalized function of (1.6): $v(y) = \frac{1}{2}\alpha v(1-v)$ has been used to simulate the two red curves, where $\alpha = \frac{\Delta p}{\eta b}$. If α is large, e.g. from higher pump rate, then the resulting parabola is steeper and a higher velocity of the flow is achieved. As can be seen the highest attainable velocity is in the middle of the chamber.

2.3 Calibration using power spectrum method

When performing experiments the trapped beads position (x,y) is detected at consecutive times. To extract the spring constant the power spectrum of (1.7) is required. The Langevin equation can be reduced by using Reynolds number (10) since $\boldsymbol{v} = const$, *R<<1* then:

$$0 = F(t) - \zeta\dot{x} - kx \ . \tag{1.7}$$

Fourier transform in the frequency domain of (1.7) gives:

$$2\pi\zeta\left(\frac{k}{2\pi\zeta} - if\right)X(f) = (k - i2\pi f\zeta)X(f) = F(f). \tag{1.8}$$

Defining *F(t)* as white noise (9), gives: $|F(f)|^2 = 4\zeta k_b T$.

Then taking the squared modulus of (1.8): $4\zeta k_b T = |(k - i2\pi f\zeta)|^2 |X(f)|^2$. Rearranging results in power spectrum:

$$P(f) = \frac{D}{2\pi^2(f^2 + f_c^2)} \tag{1.9}$$

where P (f) =2|X (f) |^2 [(4)] and most importantly the corner frequency $f_c = \frac{k}{2\pi\zeta}$.

The positional data collected from the PSD is transformed into a power spectrum, which in turn can be fitted to a function similar to (1.9) whereby we can get the corner frequency and in the end spring constant. The linear relationship between the signal from the PSD in and the actual position of the bead, by similar analysis by eq. 1.3 a

conversion factor between the singal and position can be found from the distribution of the position.

Figure 6 A basic conceptual illustration of the detection system used. (4)

Figure 6 illustrates the laser light is propagating in the z-direction, first through an objective where it gets refracted. A bead is present at or near the beam waist. The condenser recollects all the light where after it hits the exposure region, which consists of small units of detectors each able to register voltage differences. When the bead moves at the beam waist, the intensity collected by the condenser changes. The change in intensity is caused by the scattering of the beam by the bead. The change in intensity is a change in photons hitting the region. The figure tries also to illustrate the importance of focusing the condenser correctly so all the light is collected.

2.4 Data analysis

A quick recap of the drag and gradient force working on a bead, which should facilitate interpretation of acquired data. First section beings with positions of a bead and ends with a corner frequency.

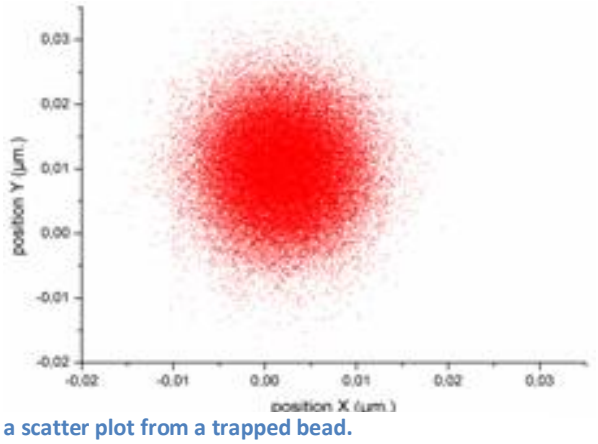

Figure 7 illustrating a scatter plot from a trapped bead.

The first plot shows the position of a trapped bead. As can be seen the bead the bead is confined within a circular area.

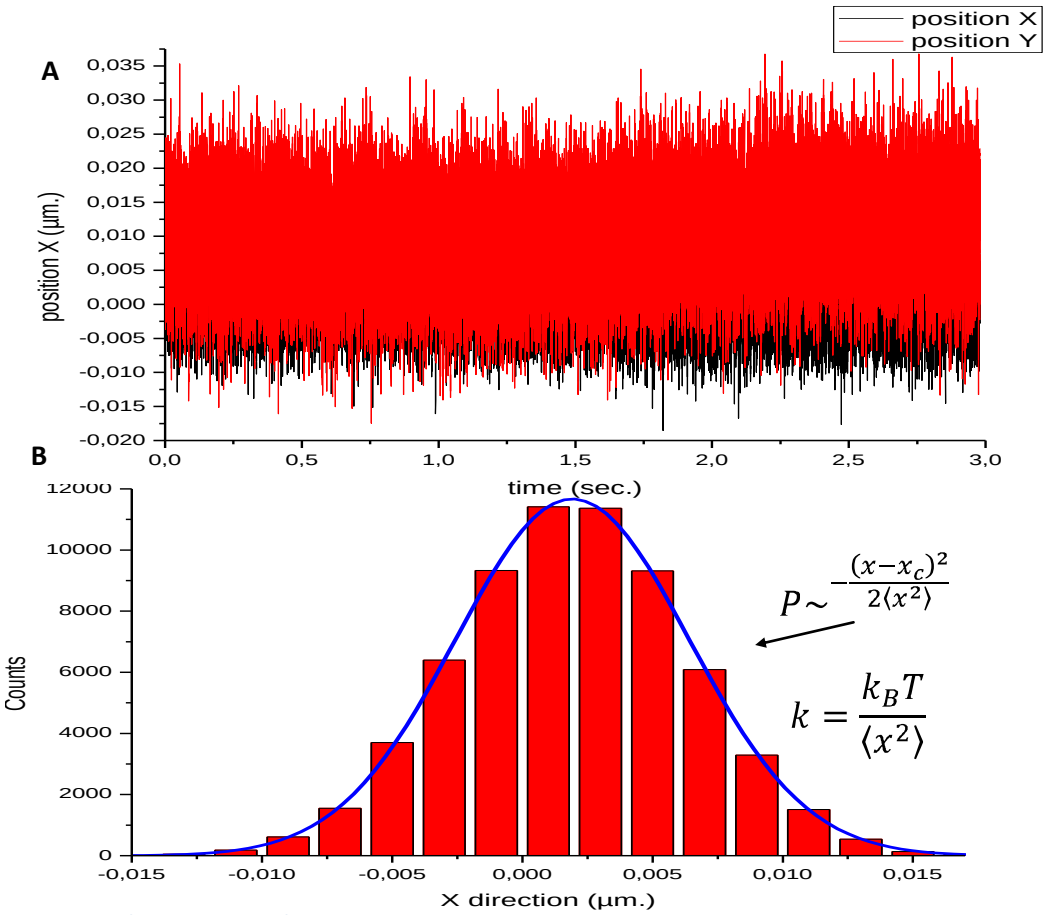

Figure 8 A) A timeseries B) Histogram of the position

A time series of the movement of the bead in Figure 8 A shows that it resides most of the time near a certain mean, whereas the rapid oscillations are illustrating Brownian motion.

Figure 8 B is a histogram of the position. Here it is seen more clearly, by the peak, that the bead is concentrated around some mean. One can interpret this mean as being the center of the trap where the bead has the highest probability to be found.

The form of the histogram resembles a Gaussian function. It originates from the fact that Brownian motion is a stochastic process, a random process which can be characterized by the Gaussian distribution function (10) and (9): $P \sim e^{\frac{x-x_c}{2\sigma^2}}$, where x is the displacement, x_c represents the mean displacement and sigma is the variance. The connection between the movement of the bead and the Gaussian distribution stems from the Boltzmann distribution. Now the Boltzmann distribution, in this case describes the

probability of the bead being in an energy state in the harmonic potential well (13). This will result in a distribution in the form of the Gaussian distribution.

Figure 8 B shows a blue line which is the Gaussian fitted function describing the probability of the bead having a certain displacement.

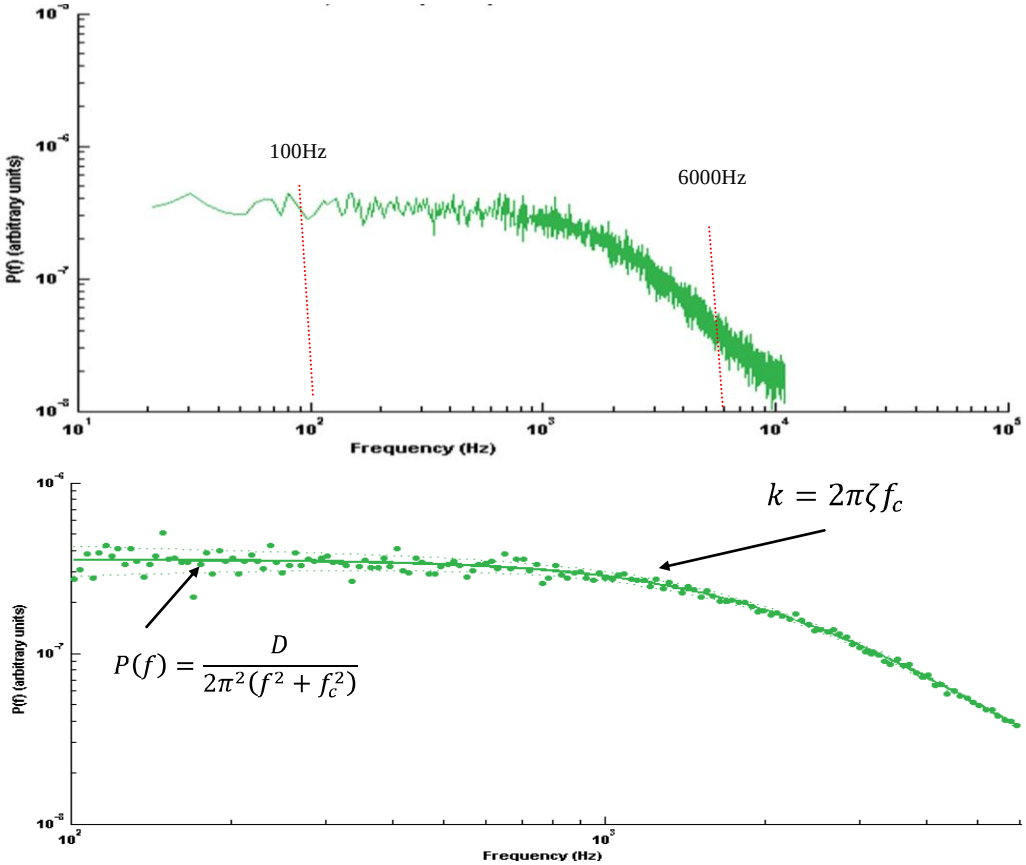

Figure 9 Fitting is corrected for: low drift and noise from electronics by cutting off frequencies below 100. And also for bead and surface interaction, cross-correlation and anti-aliasing (34) (45). Cutting off frequencies above 6000 for; noise; folding back of frequencies, since sampling rate is 11000 Hz; and unintended filtering by the detector.

Figure 9 shows a power spectrum fitting. Following eq. (1.9), the powerspectrum is nicely fitted by a Lorentzian function. To show this we turn our intention towards figure above. The point, where the graph starts to decrease rapidly, is called the corner frequency: f_c. For a Lorentzian function converging to 0 for $f \to \infty$ the following relationship must hold: $f > f_c$, this is what the graph shows with a negative slope. If $f > f_c$ then the bead performed a Brownian motion inside the trap and hardly feels the confining trapping potential. This part of the graphs is known as white noise. If $f < f_c$ it does feel the confining trapping potential.

In practice when a bead trapped with OT is observed at a time scale shorter than $1/f_c$ the resulting measurements would be interpreted as if the bead was free. Thus it is vital to observe beads at longer timescales than f_c:$\zeta = 3\pi d\eta = 3 * \pi * 10^{-3}(N \cdot s) * 3 * 10^{-6}(m) \approx 2.8 * 10^{-8}(N \cdot s \cdot m)$

$$f_c = \frac{k}{2\pi\zeta} = \frac{0.16 * 10^{-3}\left(\frac{N}{m}\right)}{2 * \pi * 2.8 * 10^{-8}(N \cdot s \cdot m)} \approx 900Hz$$

The experimental timescale was 3 seconds, which is well beyond what is required 1.1ms.

The uncertainty attached to measurements when using quadrant photodiodes are low (10).

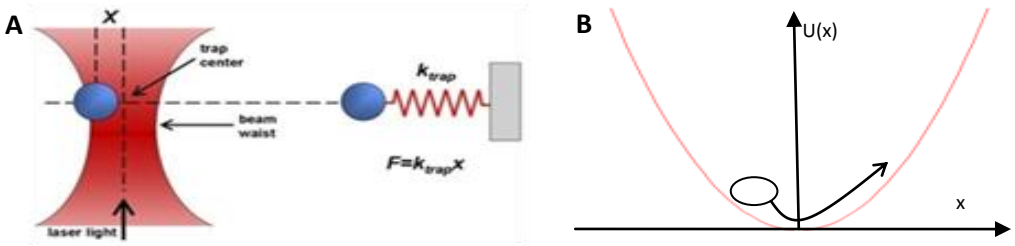

Figure 10 A) Illustrating an optically trapped bead (13). B) A trapped bead in a potential well.

Figure 10 A is of a trapped bead, whenever the bead is not in the minimum of the potential a linear force is exerted on it. The bead feels constrained to revolve around the harmonic potential well $U(x) = \frac{1}{2}kx^2$ in Figure 10 B. The steepness of the potential well and hence trap stiffness depends on the gradient of the laser beams intensity.

The laser beam has a Gaussian intensity profile (see image on page 3). A small beam waist, see image above, means that the Gaussian profile becomes less broad. Explained in Focus of laser this means more momentum is forcing the bead into equilibrium (into the center of the trap). Together with the image of a PSF in [Focus of laser], which shows the intensity; it explains a smaller Gaussian profile and beam waist (beam spot) means PSF's central peak has a higher gradient thus $F_{grad} \sim \nabla I$. A narrow potential well is achieved by increasing the gradient of the lasers intensity. This can be done by increasing the lasers intensity or decreasing the laser beams waist.

When the bead is trapped and a flow is present, the bead's relative velocity v with respect to the water is parallel with the drag force $F = -v\zeta$.

There are two considerations. One is the overall or major shift in the beads position due to drag force. The other is the restriction in Brownian motion around a certain equilibrium position. In Figure 11 A) there is no flow and the situation is as Figure 10. Figure 11 B) has a flow present which results in a drag force is imparted on the bead which makes it shift position a certain amount, shown in Figure 11 C). A new equilibrium is reached when the trap made by OT is just as strong as the force exposed on the bead by drag force from the flow, $F_{drag} = F_{spring}$: $k(x + x') = \zeta v$. That results in a new effective spring constant: $k = \frac{\zeta v}{\Delta x}$ and hence a new effective potential: $U(x) = \frac{1}{2}(\frac{\zeta v}{\Delta x})x^2$, assuming that the new effective trap is still harmonic, x is the new equilibrium position, with a higher spring constant. At higher velocities the harmonic potential well gets steeper, and the Brownian motion is more restricted.

The effective potential does not necessarily have to be harmonic.

By trapping a bead and increasing the flow rate, it should result in a higher corner frequency for the reasons given above.

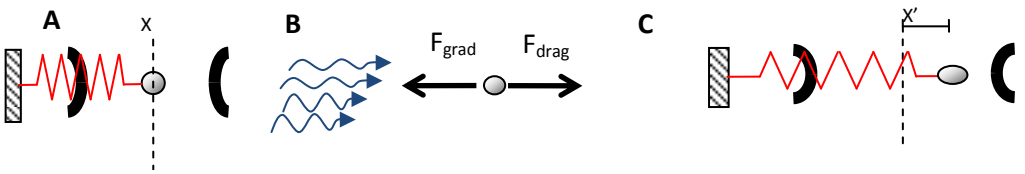

Figure 11 A)A bead in a optical trap, black lines illustrate OT and the spring illustrates the force from the trap B) Waves illustrate a flow and subsequent drag force in addition to a gradient force. C) Bead is shifted due to drag force.

Keeping a constant flow rate and moving a trapped bead towards the center of a flow chamber should also result in higher corner frequency, because of the parabolic flow profile.

2.5 Instrumentation

In this chapter a short description of the optical tweezers setup is given, followed by additional descriptive information about the most important components.

The experiments were performed in the main optical tweezers lab at setup 1, where the microscope is a Leica model and inverted, a schematic illustration below depicts the setup. Only components used will be explained.

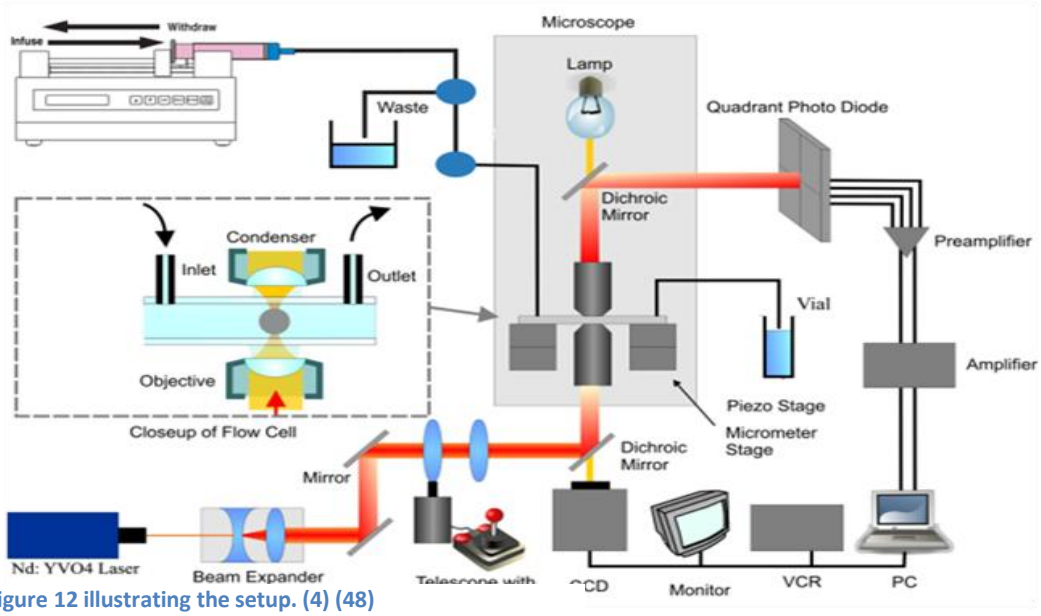

Figure 12 illustrating the setup. (4) (48)

The laser beam is generated by a diode-pumped solid state laser. The gain medium is an yttrium orthvanadate(YVO4) crystal doped with neodymium(Nd).

Figure 12 depicts the entire setup. The beam goes through a beam expander. The laser beam passes through the objective. It converges inside a micro fluidic device. A condenser collects the light. The voltage difference signal is sent through different electrical component where it gets amplified and is stored on the computer. A lamp above the second dichroic mirror serves as a light source for a CCD picture. The chamber can be moved by the micrometer stage.

The fluid system illustrated in Figure 12 is the pump, tubing, chamber vial and waste container. The blue circles represent valves. The Harvard Apparatus pump 11 pico plus is a syringe pump. The pump is operated with accompanying software executed through Labview via a serial connection to a computer. The motor drives a lead screw which makes the syringe withdraw or infuse, with a constant non-pulsating rate of flow and a constant pressure difference over the chamber. The pump is used with a 3mL syringe restricting the highest flow rate to 150 µL/min.

The chamber is formed by two coversglasses: bottom is a thin coverglass and top part is a thick coverglass with drilled inlets see image above. They are held together with premelted parafilm. Before inserting the parafilm a section of it is carved: 40mm by 5mm, which is where the experiments are performed.

Ethanol was used for cleaning in general, including tubes, chambers and the pump's syringe. Sections of the tubes were pinned down to avoid any external disturbances. Disturbances would be in the form of low frequency oscillations and sudden release of pressure.

2.6 Data presentation

To test the expected laminar flow profile created by the pump I performed experiments meant to show flow rates parabolic dependency on the height of the chamber. Measurements were acquired by trapping beads at different depths in the chamber with constant flow rate.

One bead was captured, and the chamber was flushed. The detector was aligned, so its center conquered with the beads position, with the help of the oscilloscope.

At each height the flow was turned on and a measurement was taken, lasting 3 seconds. This was repeated three times. Then the pump was stopped, when sufficient time had passed by, so that the no flow was deemed present, the valves were closed. The valves were opened again and the same flow rate was applied. Again three control measurements of 3 second were done to show reproducibility.

Two diagrams are presented in Figure 13. Both diagrams show force vs. height. Horizontal axes are normalized by chamber depths, by dividing with the maximum chamber height. The bottom of the chamber is represented with 0 and the top by 1. Vertical axes scaled with the spring constants given in piconewton pr. nanometer. The plotted points are an average of 3 measurements, and the error bars their standard deviation. Some measured points have been omitted, because the beads would reside outside the field of the detector.

Bead size 3.04. Flow is in the x-direction. The two diagrams have 2 curves each. The red curves represents measurements acquired with flow, the black curves are the control measurement with flow. All four curves have highest values at around 0,5 and lowest values near 0 and 1. Curves (x-direction): span around 0,0196 to 0,022 pN/nm. Curves (y-direction): span around 0,017 to 0,0205 pN/nm. The detector was initially aligned and centered with respect to the trapped bead, when flow was not present. Larger beads would move out of the field of detection.

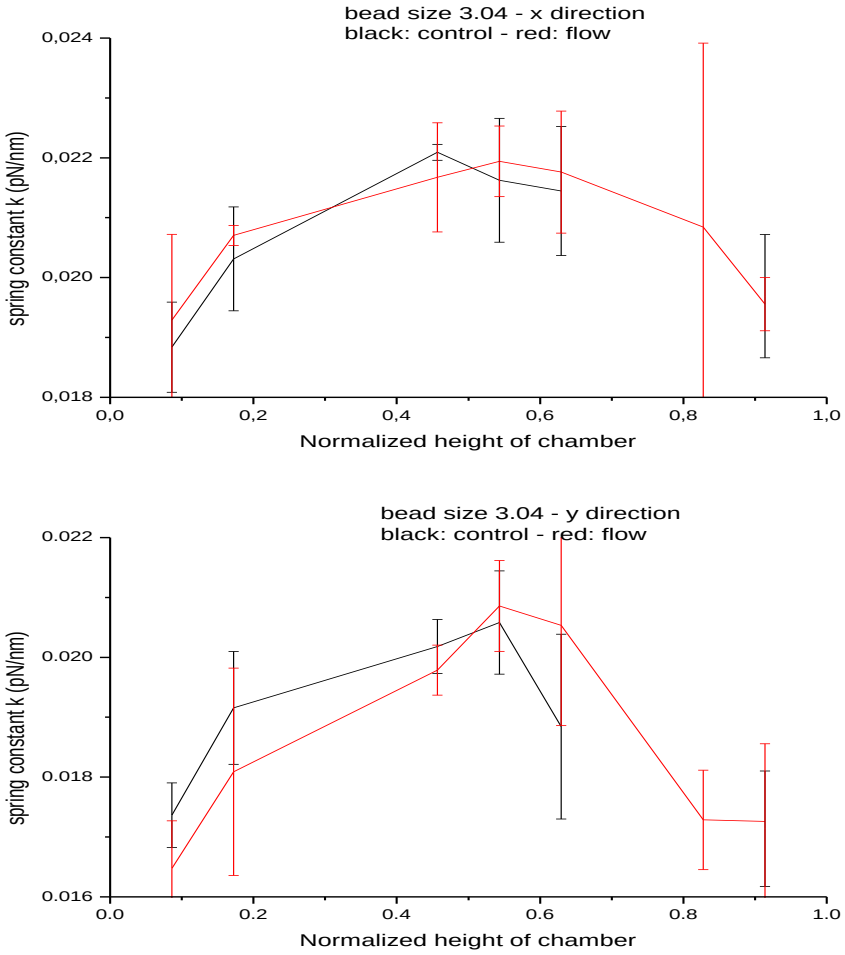

Figure 13 Red curves are before closing the valves, control flow is after opening the vales.

Both curves in each graph show same parabolic trend trends.

2.7 Summary

The first set of experiments proves that it is possible to measure the change of trap stiffness, caused by the parabolic velocity flow profile, using colloids with optical tweezers. Data collected for trap stiffness parallel to the flow was expected to be parabolic form since flow velocity should by highest in the center of the chamber $v(y) = \frac{1}{2}\frac{\Delta p}{\eta b} y(h-y)$. Data collected for trap stiffness perpendicular to the flow direction should have been constant, showing independence of height. Reason would be that there is no flow in the perpendicular direction and hence no drag, including no parabolic flow profile.

It is hard to disseminate a distinct difference when comparing spring constant for flow and without flow keeping in mind their standard deviations. The overall forms of the curves are the same taking into consideration the standard deviations. This shows reproducibility and whatever 'wrong' seems to be deterministic e.g. mechanical. Most likely something was 'defective' with the chamber, since the other experiments do provide some meaningful data interpretation.

The data shows, a relationship between force and height, with reproducibility and a concurrence with the theory. The drag force is highest in the center of the chamber because of the parabolic velocity profile, and as known from theory the drag $F_{drag} = -v\gamma$ results in the trap being stiffer $k = \frac{\zeta v}{\Delta x}$. Thus all force measurement values, parallel with the flow, are higher than the ones perpendicular to the flow. No drag force is acting perpendicular to the flow direction, making the trap unaffected. As was explained in the theory the potential well is steeper in the direction of the flow, whereas it is relatively less steep in the perpendicular direction. With a non-symmetric trap the bead will move more in the perpendicular direction, and thus the trap stiffness measured should be less.

One problem is with the supposedly independent direction, which is perpendicular to the direction of the flow, showing a dependency of drag. The valves were closed so no apparent flow was present. This was checked by observing a freely moving bead. It did not have any bias. The curves should have been constant with respects to the height.

Uncertainties are still high, although there are clear tendencies i.e. difference in the values found at between the center of the chamber 0,5 and the edges 0;1.

Chamber design changed by having syringes go through the side of the chambers, instead of drilling holes through the coverslides. Length of the tubing was also reduced, and the valves were removed. Other precautions were taken to reduce noise to the system.

3 Cover Glass

Improving the optical trapping strength of optical tweezers.

Manufacturers produce objectives specified to be used with wavelengths in the visual regime while trying to reduce artifacts. Using them in optical tweezers, which is based on infrared light, may not be optimal. By changing the cover glass collar correction (CGCC) settings, experimental data will explain what the optimal correction will be for a strong trap. This section will present the investigation of what happens, when an optimal CGCC value is not used. The optical trapping strength is dependent on the form of the intensity gradient and thereby also aberrations [Focus of laser]. The maximum trapping strength is achieved when the aberrations are minimal. Experiments were performed to find: A: the relation between the trapping strength and aberrations. This was done by observing the trapping strength while adding aberrations. B: Show a relationship between the CGCC settings of the objective, when using different thicknesses of cover glasses.

3.1 Aberration

Not all of the rays from an object will converge to one point when they transverse through an objective, notwithstanding the diffraction limited spot [Focus of laser]. One reason can be aberrations. The effect of aberrations can be minimized see Figure 14.

3.1.1 Spherical aberration

The Gaussian lens equation is derived by interpreting the rays arriving from an object as being paraxial rays (14) (15) (16). The angles are defined by the incoming rays to the normal of the lens. Approximating the angles as being small enough, it is possible to equating $\cos(\theta)$ and $\sin(\theta)$ with their second order Taylor series: $cos\, x = 1 - \frac{x^2}{2!} \ldots$ $sin\, x = x - \frac{x^3}{3!} \ldots$ This approximation is sufficient for waves in the paraxial regime, but this in turn sets a restriction on describing rays interacting with the lens' periphery.

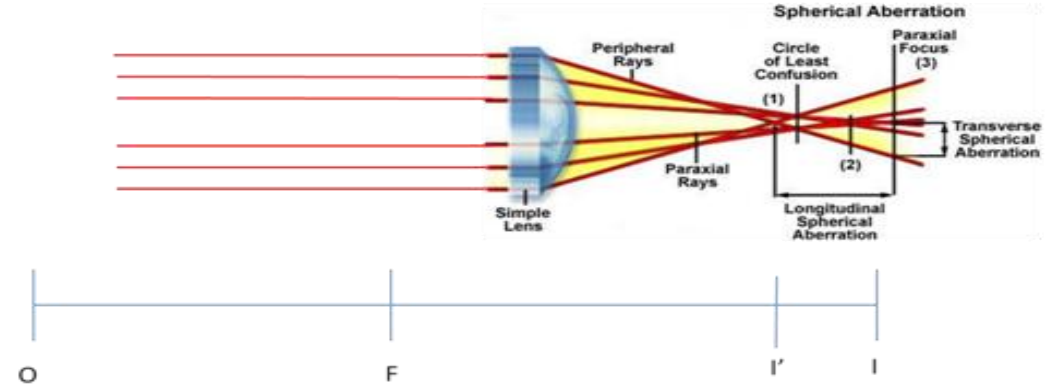

Figure 14 : The picture shows spherical aberration where the rays are travelling from left to right. Rays near the periphery of the lens converge at (1). Rays in the paraxial regime are converging furthest away at (3). Rays in between these areas converge near (2). Longditudinal spherical aberration shows the "smearing" out of the beam waist in the z-direction, and transverse spherical aberrations shows a wider beam in the x-y plane. (47)

By addition of the third order in the Taylor series expansion, it is possible to add an additional term in the Gaussian lens equation (14): $\frac{1}{O}+\frac{1}{I}=\frac{1}{f}+h^2k$, height h of the incoming rays intersecting the lens at the optical axis. The equation describes how the rays at the periphery are refracted more than those which are near the optical axis; hence the former ones converge closer to the lens' than the latter ones. Spherical aberration manifests two planes, this means that either the outer edges (1) or the central part (2) of the object is projected properly, an alternative is choosing the plane between the two "best" planes. To completely remove the converging rays from the periphery a smaller aperture can be used, this would result in image detail being lost. A more satisfying option to reduce spherical aberrations is by introducing a combination of lenses, whereby all rays converge to one single point. This can be done with a meniscus lens, hemispherical lens, a cover glass, and immersion medium air, water or oil. Spherical aberrations are introduced when light travels from one media to another see Figure 14**.**

3.2 Objective

In this section features of the objective will be explained. The objective used has a magnification of 63X, and is used with water as the immersion medium. It includes the ability (CGCC): 0.14 – 0.18 mm thick. Numerical Aperture (NA) for this lens is 1.20.
Turning the reader's attention to (CGCC): In some objectives a mechanism is included to correct for deviations of the cover glass thickness.

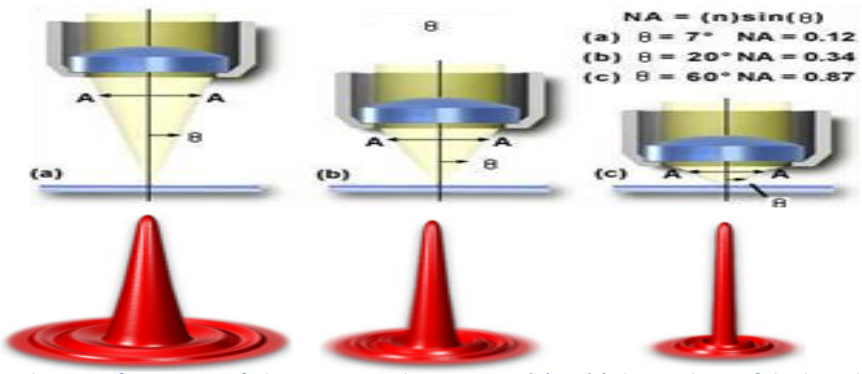

Figure 15: Three configurations of objectives are shown. From (a) to (c) the gradient of the laser beam, seen here as the yellow cone, increases with NA. **(15) (49)**

To keep aberrations as low as possible and have a high numerical aperture (NA), the configuration of internal lenses of an objective are designed to work optimally with specified immersion mediums and cover glass thicknesses. If the cover glass thickness is different than what is proscribed, it will lead to spherical aberration (17). The CGCC changes the internal distance of some of the lenses in the objective, which in turn also changes the focal point, so the objective correlates with the cover glass thickness.

NA is a measure of the amount of being of rays from a sample which an objective can transmit. If the object is a point source the lens is in effect (re)collecting the rays of a point source. The resolution can be described by (18): $r = \frac{1.22\lambda}{NA\ objective + NA(condenser)}$. If the objective is placed near the source point, a certain amount of rays will be collected, placing the objective at a further distance would mean those rays emanating with a high degree of divergence will not be captured by the objective. This will amount to a loss of trapping stiffness see [Figure 15]. This is the essence of NA which is described as (19): $NA = n_m \sin(\theta)$ n_m is the refraction index of the medium between the objective and the cover glass. θ is defined as being the angle acceptance. A high angle gives a high NA, which is consistent in having the objective close up. Since θ has a maximum value 72 a high index of refraction is desirable, water has 1.33.

3.3 Experiment

Distilled water was used as immersion medium. A concentrated solution of beads was diluted 1/million in distilled water.

A chamber was made by sticking double sided tape along the two long sides of a thick cover glass thus making a corridor. The chamber was covered by a thinner cover glass, which would be facing the objective. A diluted solution was injected into the chamber via the capillary force caused the solution fill the entire cavity. Last step was to close the chamber with grease. The thickness of the tape was 80-100µm. The condenser was used with oil as immersion medium. To get the optimal condition with respect to the quadrant photodiode Köhler illumination was used. Measurements were acquired by

QPD. The laser output power was 200mW. The laser is polarized in the x-direction. The results of experiments are given beneath.

3.3.1 Results

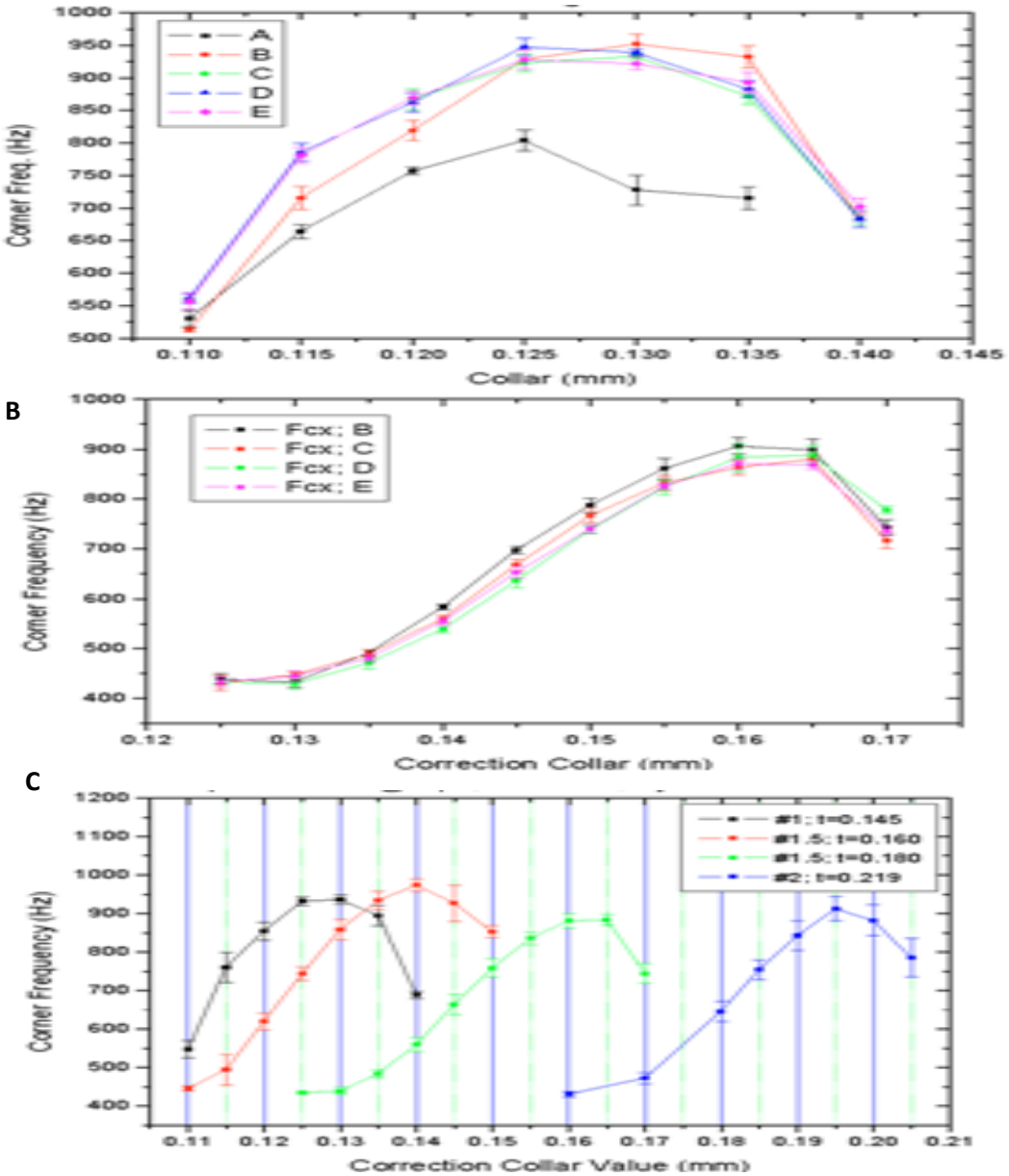

Figure 16 All figures show trap strength in the x direction vs. collar values for different coverglasses. Laser power output: 200 mW; bead diameter 0.8 µm polystyrene; Water immersion objective; At depth of 10 µm. A) A to E are the five chamber, where the chamber holder for A was faulty. B) Data for coverglass # 1.5 C) Data for all four different thicknesses of coverglass.

Experiments were done with four different thicknesses see Figure 16 C), each one with four chambers and consequently four beads. Experiment consisted of changing CGCC from highest to lowest value. Polystyrene bead diameter: 0.80µm ±1%. Four beads were deemed as sufficient for statistical weight since the low uncertainty of the bead diameter meant that the differences in beads were low.
Figures show x-axis values representing CGCC in mm and y-axis corner frequency (f_c) in *Hz*. Figure 2 a, shows five curves each representing one chamber/bead. Each point is based on averaging five calibrations pr. bead, notice small error bars. Curve "A" differed substantially because of an uneven sample holder. Subsequently only four chambers were used. Figure 2 b is representing four curves where a thicker cover slide was used. Figure 2 c is showing four curves each based on an average of four curves for each thickness. All of the curves increase from lower CGCC values and have a steeper decreasing gradient after reaching peak values. Each maxima shift's with increasing CGCC value and correspondingly thickness. For thinner coverglasses (cg) the maximum f_c is higher, which might be because the laser light is refracted less, and less laser power output is lost.

There was a sharp transition between the highest acquired CGCC value and not being able to trap a bead. Whereas at the lowest CGCC values a bead would be loosely trapped, at the slightest external force the bead would escape, and the bead could only be moved carefully. Lower values of CGCC allowed the bead to be trapped but for a short time span, not long enough to acquire data. Whenever the bead could not be trapped, it would be pushed out of focus, when trying to capture it. The highest difference in F_c is about factor 2. Apart from $F_cx < F_cy$ both directions show the same trend. The decline of the curves at a slower pace indicates that the objective is more tolerant towards changes in CCGC fest of the peaks.

There was also a clear visual difference of the bead from the lowest and highest CGCC values. The beads outer lying dark ring became larger, indicating that the bead had shifted focus away from the objective. Another observation was the bead could be trapped in the second potential. This was noted by a shift in the beads focus away from the objective, a weak trapped bead and a visual shift in the X-Y plain.

3.4 Discussion

An optimal convergence point would be one without aberrations. By using cover glasses with matching CGCC values minimizes aberrations. Peak CGCC values showed the highest F_c which can be translated into a strong trap.

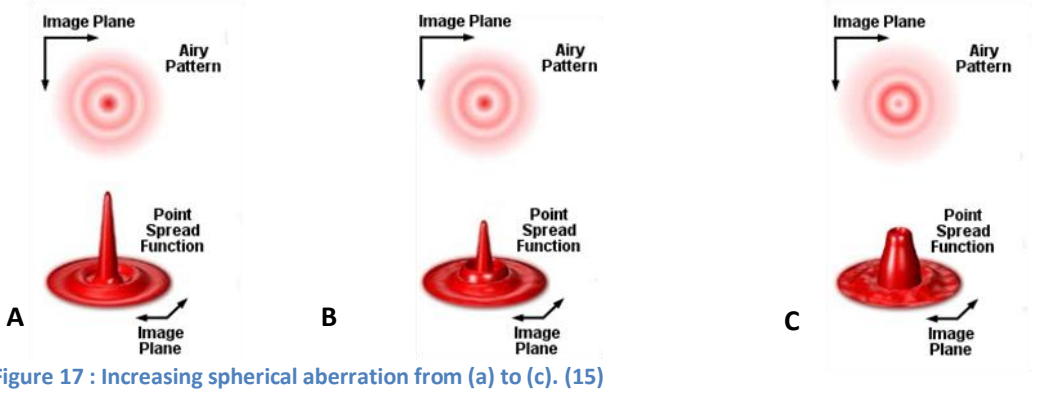

Figure 17 : Increasing spherical aberration from (a) to (c). (15)

A strong trap is when Gaussian intensity profile has a high gradient. Experiments also showed us when moving away from, what one might perceive as the optimal correlation between objective and cover glass thickness, the F_c decreased. This must mean an unstable trap and a broader profile. Choosing an incorrect CCGC value would result in introducing aberrations. Spherical aberration will be present in the experiment since infrared light was used, and spherical aberration is not corrected for light in this regime. It seems that the reason for getting low gradient (F_c values) is because of aberrations [Figure 17]. Spherical aberration widens the focus point which translates into a bigger the focal region where the intensity is present. Spherical aberration would move focus points along the z-axis and less in the x and y [Figure 14]. Experiments done (not shown) with larger beads at lower laser power resulted in the bead oscillating in the z plane, when at the lowest CGCC value. The reason might be a lower restoring force compared to forward scattering. But the bead moved less in the X-Y plane than the Z direction, which must mean that the focus has been 'extended' along the z direction. Indicating spherical aberrations, and means aberrations affect the trap more in the z direction than in X-Y plane.

When beads slipped out of equilibrium, the restoring force was not strong enough to counter the forward scattering force i.e. too much aberration. Aberrations definitely alter the geometry of the trap and in that effect also the force distribution on trapped beads.
All of these observations are consistent with experimental data.

3.5 Summary

Since objectives are not corrected for wavelength in the infrared, spherical aberration is present. It is seen as weakening of the trap. Experimental data showed a maximum f_c can be found. As the CGCC values were changed from the optimal value f_c began to decrease. This was seen as adding aberrations. At certain values the aberration was strong enough to reduce the Gaussian intensity gradient of the laser, thus making the trap unstable. Each thickness of coverglasses had their own corresponding CGCC value where the trap was strongest and weakest. The thickness of coverglass does not seem to change the effect of aberration, since the curves have more or the less the same form. That is because the condition to optimize is the same. Both $f_c x$ and $f_c y$ are affected by aberrations; there are not any large discrepancies except at peaks. Trap stabil-

ity is sensitive to aberration, and either aberrations are corrected as f_c increases or aberrations are added and f_c decreases.

Figure 18 shows the horizontal axis depicts the real coverglass thickness measured by a micrometer ruler. The vertical axis is the apparent thickness measured by laser reflection or the optimal collar value. The points on the red curve are the coverglass thickness measured with a micrometer ruler (real) vs. those measured by laser reflection (apparent). The points on the black curve are the thickness measured by micrometer vs. the optimum collar value. Both change linearly with a slope within 5%. There is clearly a relationship between laser reflection thickness and the optimal CGCC value.

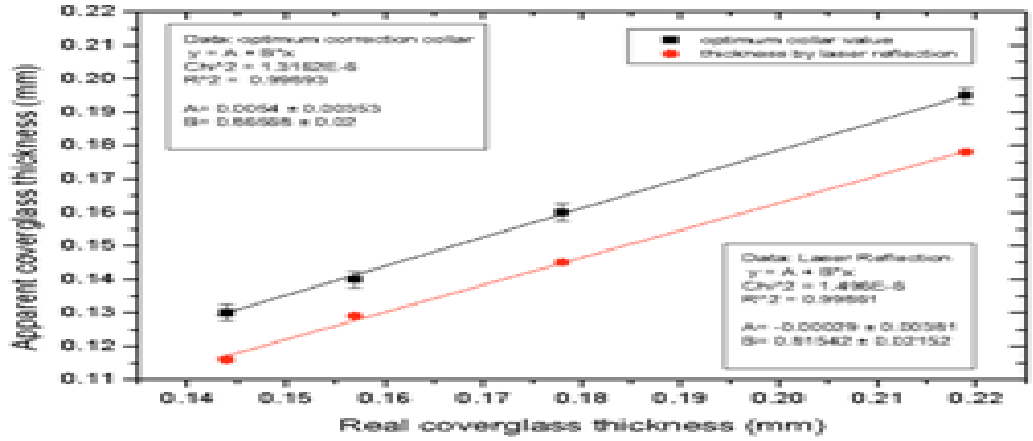

Figure 18. Both data sets have been fitted to linear functions, see boxes.

The optimal collar value could now be used for other experiments.

4 Deoxyribonucleic acid (DNA)

Hereditary information for humans and alike is stored in DNA. Four types of nucleobases are found in DNA, the sequence of which is the information. DNA is present inside cells; the former is replicated during the division of the latter. DNA can be unwounded by enzymes which also transcribes the information into a complementary strand. This strand is then translated by another enzyme into a specific sequence of amino acids which constitute a corresponding protein.

Various reasons can lead to structural changes of DNA. Some toxic chemicals bond covalently or electrostatically with DNA causing damage by inhibiting replication and transcription. Others work indirectly e.g. by inducing the creation of reactive oxygen species (ROS). ROS in turn, due to oxidation, break strands and corrupt the information leading to cell death or mutation; which can have serious consequences in the form of cancer.

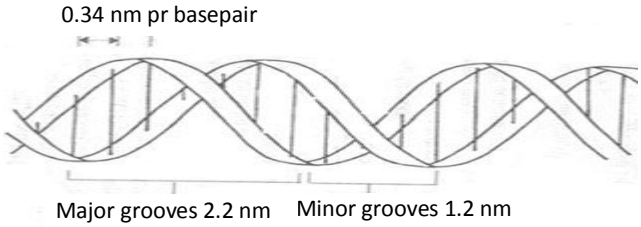

Figure 19: Illustration of dsDNA model (50) (51) (52). Synthetically formed dsDNA is used in the experiments: diameter ca 2 µm (35) length 1.1 µm.

Watson and Crick postulated the form of a DNA molecule being double stranded (dsDNA) and twisted in a helical fashion, see Figure 19. The figure illustrates the dsDNA as being thin compared to its length. It also shows sections over which double helix completes a turn. Within this repeating pattern the groves created have uneven widths. DNA is further segmented into basepairs. Each base in turn consists of a nucleotide: a sugar and a phosphate group and either one of four different nucleobases. Nucleobases are specific pair wise compatible through hydrogen bonds. Each strand has an end with a free 3'OH group while the other end has a 5' phosphate group, both strands run counter. The exposed backbone consisting of sugar and phosphate groups is polar, hydrogen bonded and negatively charged. DNA molecules can be in different families of conformations, the most physiologically common is called B-form. Its conformations are due to its flexibility which depends on ion concentrations. Information regarding conformations will be elaborated in section [Explaining the DNA model.].

4.1 Tether formation

OT creates the opportunity to study individual DNA molecules. By measurements of "mechanical" forces, through the ability to perform force extension experiments, on single dsDNA. Probing the molecules elastic properties over a range of small forces (pN) and displacements (nm), gives insight into intramolecular interactions. Assuming in such a case the DNA's internal dynamic process is following a path of equilibrium when stretched. If the DNA complex has been altered, so that it follows a different equilibrium path, its internal energy enthalpy has changed. In this case the process indicates intermolecular interaction, in the scenario if Figure 20. In either case dsDNA's structural configuration is addressed through its persistence length which relates to DNA's entropy. As mentioned above ions do also influence the dsDNA configuration.

How would one do experiment on single dsDNA? What would the experiments look like? Analog to probing a spring's characteristics by F/X =K, in a similar manner applying a force to measure a displacement is done by actually stretching a dsDNA. This part is in essence what roughly the whole experiment boils down to. A strategy illustrated schematically in Figure 20:

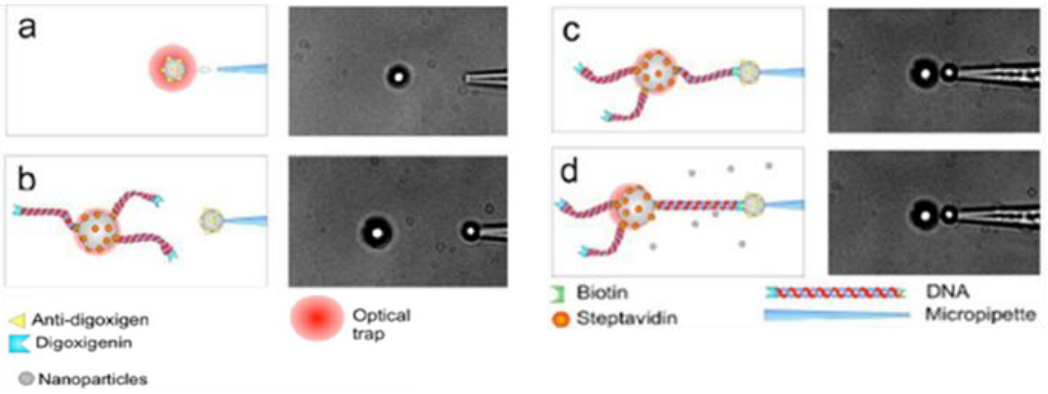

Figure 20: Experiments are carried out inside flow chambers, in solutions with and without C_{60}. Small bead 2.1 µm, large bead ca 3.09 µm. Protocols are in [Appendix]. Not shown: A steady flow of C_{60} is flushed into the chamber and capillary pressure created current. Picture is a top view in the x,y plane, view from the streamed picture from computer. (4)

A. A bead is trapped by a laser and subsequently moved in the vicinity of a pipette inlet. At a sufficient distance the capillary force is strong enough to suck the bead to the mouth of the pipette.
B. A larger bead is trapped and subsequently calibrated, where after it is brought next to the small bead.

C. The dsDNA attaches specifically to the other bead thereby tethering the molecule.
D. The pipette is moved away from the large bead in the process stretching the dsDNA, and relaxing by subsequently moving back. The procedure is repeated preceding introduction of a solution with C_{60}.

Stretching-relaxing the dsDNA induces a force on it, whereby a force-extension relationship is achieved see Figure 35.

At point "B" the optimal condition is to have a tether form directly between both beads. To ascertain this both beads are visually aligned by means employing the zoom lens, obtaining a resolution of 0.08 nm pr. pixel, and digital zoom. Alignment in the plane is done by centering the beads with the help of digital markers. Throughout a beads dept it has a distinct pattern, radius and thickness of the white ring. By comparing these features their relative height can be assessed.

Fishing for a tether: The laser power output is lowered so the large bead makes a less confined Brownian motion and is more likely to approach the small bead. The pipette is moved towards the large bead in steps of 50 nm and each time being pulled back. Both procedures employed avoid rupture of a bond and beads colliding with subsequent multiple tethers, it is also easier to detect bonds. Detection of a tether is observed when its Brownian motion is restricted and when it is pulled with the pipette, eventually out of the trap. The released large bead will perform biased restricted Brownian motion around the small bead.

4.1.1.1 Molecular biology: Handles, multi tethers & broken.

The ends of dsDNA are originally sections of unpaired and dissimilar base sequences. Molecular pairs of handles, each handle with base pairs complementary to one end of dsDNA, are added to the dsDNA's ends. One end is attached with biotin which adheres to streptavidin coated bead. The other end has the antigen digoxigenin (Dig) which pairs with its complementary antibody anti-Dig coated bead. DNA molecules are incubated with streptavidin coated beads over time where after they are bonded [Appendix B.]. In "C" the free end of DNA finds an anti-Dig binding site on the other bead, it would take within minutes to form. Before each experiment a fresh batch of DNA grafted beads were produced. This was due to time dependant "degradation". When used the same day a tether would generally form within minutes. If a batch was used after several days it would take several minutes to form a tether, and no tethers would form after more than one week.

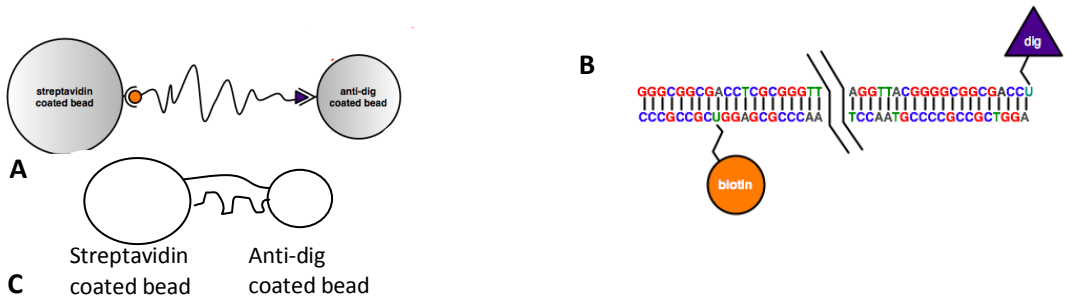

Figure 21: A) Beads are coated with streptavidin and anti-Dig handles (53). B) Only one dig linker on the DNA might be the reason for DNA-bead disassociation at higher forces (53). C) Strands represent individual DNA. One is stretched more than the other.

Multi tethering: Multiple tethers do form if both beads are in physical contact, especially if they stay like that. Tethers will avoid forming near each other due to unfavorable energy considerations. This was observed when high concentration of DNA molecules on the streptavidin coated beads resulted in multiple tethers being formed at the anti-Dig coated bead. In this case the observed trapped bead showed a very confined or non Brownian motion. To increase the bead-to-bead displacement higher forces are required than usual. What is observed is a sudden increase in displacement when holding the tethers in a stretched position or when stretching them. This might be due to one DNA tether getting stretched before the other, then proceeded by a bond breaking followed by an increase in displacement for the same amount of overall force. Rarely was it possible to disassociate both beads from each other.

Specific attachment: From loads of about 25 pN and upwards, bond breaking would be observed. This might be attributed to, as illustrated in Figure 21, only one Dig anti-Dig tethering point forming (20). Thus for experiments the stretching distance and laser power output would usually correspond to, a force less than 25 pN on the DNA. If the DNA end have had several Dig labels, then it would presumable be possible to have several tethering points, and thereby exert forces above 25 pN without disassociating the tethered DNA.

5 Carbon 60

The context of this section will revolve around the carbon-60 (C_{60}) molecule. First a short introduction to C_{60} including a description of its charge distribution, which will be relevant when describing hydration. Secondly some observations regarding aggregated C_{60} (nC_{60}) will be presented.

5.1 Introduction to the non isomer molecule

Experiments performed over a period of 10 days in 1985 resulted in the formation of fullerenes, thereof a predominantly stable molecule with an a.m.u. of 720 christened 'Buckminsterfullerene' The scientist were rewarded the Nobel Prize for the discovery (21).

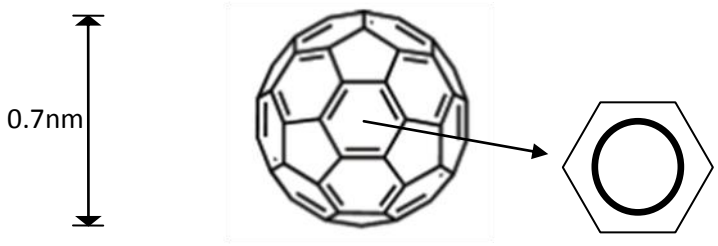

Figure 22: C_{60} a symmetric 3 dimensional closed cage molecule comprised faces of 20 hexagons and 12 pentagons, and a carbon at the vertexes (22) (54). Black circle in the close up illustrates an aromatic ring.

The fullerene consists of 60 carbon atoms in a truncated icosahedron structure. Each carbon atom is bonded to three others through, two long single and one short double, covalent bonds. Bonds between hexagons are: 0.140nm, and between hexagons and pentagons: 0.145nm. Molecules stacked as face centered cubic lattice have a nearest neighbor distance of 1.004 nm. Distance between two adjacent C_{60} molecules is thus 0.304 nm, larger than the internal carbon to carbon distance of a C_{60} molecule. At that intermolecular distance C_{60} bond to each other through weak van der Waal interaction compared to the strong covalent bonds of C_{60} (22).

The surface has an electronegative density due to π orbitals which extends outside the shell and dominates bonding properties (23). These orbitals form aromatic rings in the hexagons and increase in character as the molecules becomes more anionic (24).

The molecule's electron affinity stems from the partially filled orbitals. This means that electron rich species can react with it by transferring electrons. Although the bonds are saturated the molecule is not 'super' aromatic because of different lengths of bonds resulting in π bonding electrons not being delocalized in the hexagons. That makes the molecule not 'completely' stable but it behaves like an electron deficient alkene (25). The whole molecule can accept up to 12 electrons whereby all the electron orbitals are filled (22). Different substrate adsorption experiments have shown a variety of binding types, strengths. This includes bonding of C_{60} with alkali metals which form ionic compounds, by charge transfer from substrate to unoccupied levels (22).

Regarding this thesis C_{60} is dissolved in KD-buffer, which is a salt solution with Mg^{2+} and Na^{1+} alkali metals. A Possibility of ionic bonds might form by transfer of electrons up to

C_{60}'s saturations point: $Na_{12}C_{60}^{-12}$, $Mg_6C_{60}^{-12}$. This might affect the ionic condition by lowering its concentration. Since no change in pH levels of the buffer was observed, a change immediately in the vicinity could be a possibility (26). The ionic bonds would make C_{60} molecules more anionic. A reduced negative charged density should reduce electrostatic repulsion of C_{60} molecules and make them more susceptible to agglomerate.

Following are some noteworthy observations when working with C_{60}.

Difficult to dissolve C_{60} Figure 24.

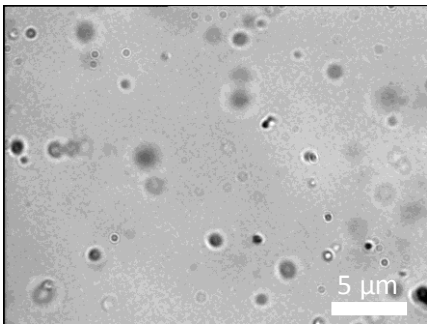

Figure 23: Image from microscope. Dark spots show nC60, by vortexing and sonicatinga a high concentration 1 mM of C_{60}.

C_{60} is initially in a powdered form when mixed in the buffer it aggregates. Reducing the initial concentration of C_{60} then sonicating and finally vortexing the solution does reduce the aggregate sizes [Appendix D.]. Figure 25 A) shows aggregates of C_{60} when high concentration of C_{60} was mixed in the buffer. This is not uncommon and there seem not a standardized protocol which solves the issue of aggregation (27) (28) (29). Although aggregate sizes are reduced they are not eliminated and single C_{60} molecules have not been reportedly observed (27).

They aggregate with wide variety of sizes and shapes: Figure 24.

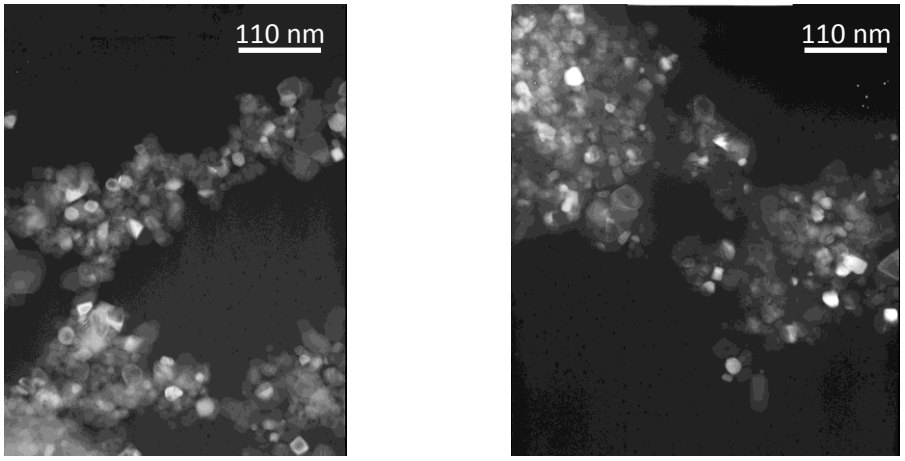

Figure 24: TEM pictures. Solution of C_{60} dissolved by sonicating, vortexing and 100 nm pore size filters.

Figure 24 shows TEM images of C_{60} mixed in KD-buffer using the protocol. Like Figure 24 A) it shows C_{60} seem to aggregate. A difference in sizes of nC_{60} can also be observed both in Figure 24 and Figure 24. But unlike nC_{60} in Figure 24 A) they seem to be below 200 nm in size, which cannot be seen through a microscope. The largest nC_{60} observed were below 0.5 µm, scarcely found and seem to be of the same size. That there are more than one distribution of sizes has been reported (27).

The shapes of nC_{60} in Figure 24 seem to vary with size. Larger nC_{60} of about 5 µm seem to be more oval, whereas smaller nC_{60} seem more around. The TEM images also shows difference in shapes some are more around whereas others are squarer. These finding concur with previously obtained results (28). Those results indicated a correlation between geometric shape and size of nC_{60}, they also found that nC_{60} were of crystalline structure.

They can be optically trapped.

It was possible to trap nC_{60}, with small nC_{60} being stable in the trap compared to large ones which could only get attracted to the trap but not trapped. Which is a feature in common with beads [Focus of laser]. Trapped nC_{60} would get knocked out by larger or smaller nC_{60}. That it is possible to trap nC_{60} indicated that they are dielectric since trapping required that they polarizable to interact with electric field from the laser.

The scarcely found nC_{60} below 0.5 µm did knock the optically trapped bead out of the trap. The trapped DNA grafted bead would have a changed pattern due to it being shifted in the trap. On closer inspection the bead would have a dark bulge, which most

likely was nC_{60}. To avoid bead being shifted or getting knocked out of the trap filters of 100 nm pore size were used to eliminate large nC_{60}.

They stick to pipette and also beads: Figure 25.

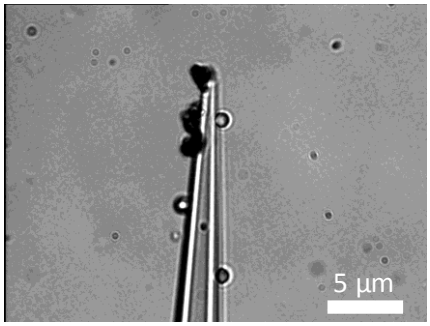

Figure 25 Picture of pipette inside a chamber filled with a solution of C_{60}. Solution was sonicated, vortexed with 1 mM of C_{60}. Anti-Dig coated beads have un-specifically stuck to the pipette. Dark mass is C_{60}.

Figure 25 illustrates a pipette with anti-DIG coated beads unspecific binding to it. The dark mass is nC_{60} which is adhered to the beads and the pipette.

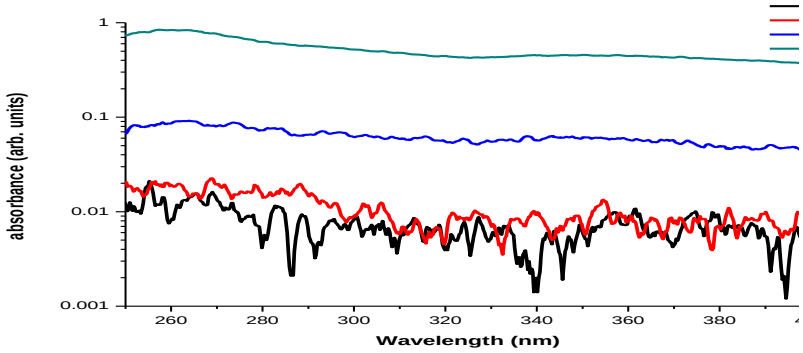

Figure 26: Absorption spectrum of C_{60} at different concentrations.

UV-absorption spectrums were taken for four different concentrations, C_{60} absorption wavelength is at 350 nm. At concentration of nM the spectrum has too much background noise meaning the concentration was too low to detect C_{60}. Subsequently it was decided to just use a concentration of 1 µM was used for the experiments.

5.2 Dissolving C_{60} in H_2O

This section explains what the conformation of C_{60} might be in water. How this might affect DNA will be elaborated on in [Discussion: bare dsDNA]. This is a theory proposed by (30) (26) (1).

It is seemingly trivial but yet still not conclusively clear as to how exactly C_{60} and water interact. Two descriptions of theories are presented (30) (26). First case emphasizing on the hydrogen bonding through the aromatic rings, the other one on attracting a hydrated layer on C_{60}. In both cases molecules end up having a negative layer.

Electron clouds of π bonds above the hexagonal plaints of C_{60} can form hydrogen bonds with water donating hydrogen atoms. The hydroxyl of 20 water molecules should be able surround a C_{60} molecule by positioning centrally and vertically over the 20 aromatic rings, Figure 27. Additional layer of 60 H_20 can bind via hydrogen bonds to these 20 molecules to further form an eventual larger icosahedral water cluster $C_{60}(H_2O)_{80}$. This results in a negative charged surface, via weak hydrogen bonds.

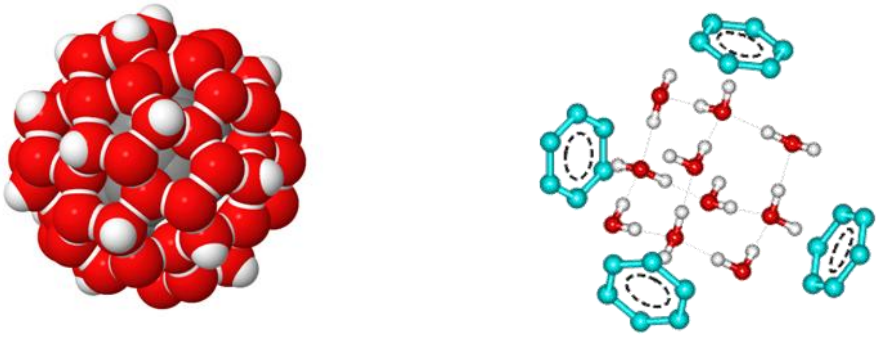

Figure 27: A) $C_{60}(H_2O)_{80}$. Icosahedral water cluster. Inner most $(H_2O)_{20}$ dodecahedrals cage similar in size of C_{60}. B) 10 H_2O part of a water network, in between hexagonal rings of 4 different C_{60} molecules.

Electron density in C_{60} molecules is high in hexagons and in between carbon bonds. Thus allowing the carbon atoms to be electron deficit. This would allow lone pair electrons from oxygen to interact with carbon atoms: C-OHH. It would be possible for these additional water molecules to be situated under the outer icosahedral water shell, and be linked to it by hydrogen bonds. Furthermore ionization of C-OHH results in hydration around C_{60}, which will increase the negative charge of the surface of C_{60} in addition to making the solution acidic. Hydrogen ions associate in water around shell. Up to 6 electron donating hydroxide ions can add to the electron density of the aromatic hexagon rings resulting in a stronger OH – π electron hydrogen bonding: $C_{60}(OH^-)_6(H_2O)_{80}$. Clusters of 13 C_{60} of size 3.4 nm have been detected, with hydrogen bonded H_2O filling the

spacing between the C_{60} molecules (30). Ions destroy expanded water networks result in coagulation of C_{60} (30). The hydrogen bonds are stronger than the OH-π bonds, and there will likely be weak van der Waals forces in between the C_{60} molecules.

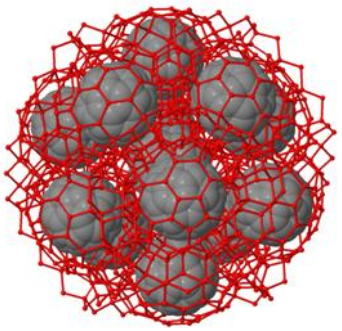

Figure 28: A cluster of C60. $C_{60}(H_2O)_{1020}$: Diameter of carbon clusters 3.5 nm (30). Hydrogen atoms have been omitted.

Another possibility might be of C_{60} having the ability to react with water molecules and form a complex with hydroxyl ions through its electron affinity trait. Possible reaction would be as follows. C_{60} molecules electron accepting ability might attract lone pair and as a result draw oxygen atoms towards its surface, subsequently polarizing the H_2O molecule. One Hydrogen atom from the attracted H_2O molecule would form a hydrogen bond to an OH^- from the aqueous solution and create a H_2O molecule. End result would be C_{60} acquiring a negative charge by an adsorption of hydroxyl ions (26).

5.3 Discussion and summary.

Experiments seem to indicate a C_{60} - H_2O complex, C_{60} hydrated (31) layers and sizes of 3.4 nm aggregates (32). These formations have been theoretically (33) evaluated. In these experiments organic solvents where used to dissolve C_{60}. These organic solvents mitigate aggregation when compared to dissolving directly in water (27). Another issue is organic residue at the C_{60}, which have been proven to produce a more toxic effect, than when solvents have not been used (28). Subsequently use of organic solvents where avoided during experiments.

C_{60} molecule has been detected in nC_{60} form. They must be polarizable since they can be optically trapped, and it is expected that C_{60} molecule as a varying electron density on the surface. This in turn can lead to it being surrounded by a water cluster.

Thus far it is possible that a C_{60}'s electron affinity attracts Mg^{2+} and Na^+ and form of an anion which might make it more susceptible to interact with DNA, since electrostatic repulsion is decreased.

Other experiments (26) have shown that nC_{60} have negatively charged surfaces and are stable due to strong electrostatic repulsion. These experiments have also shown that the electro negative charge decreases as concentration of H^+ increases. Through titration experiments it was found that OH^- is the ion which determines the negative potential of the surface.

Even with a negatively charged surface it was observed that nC_{60} does adhere to the glass pipette, the anti-DIG coated beads, and also the DNA grafted beads. Which leads to the possibility that nC_{60} might be able to attach to DNA.

It might be possible that Mg^{2+}, Na^+ and H^+ can act as mitigating agents to the electrostatic repulsion and subsequently increase possibility of interaction with the negatively charged DNA backbone.

6 Force extension curves

To recapitulate the experimental setup: A dsDNA is tethered in-between two beads. The pipette mounted bead is moved by the piezo stage relative to the other bead, which is held stationary in the optical trap. As the pipette is displaced an increase in the distance between the beads generates a force on the dsDNA. Measurement of the trapped beads displacement, due to a force response from the dsDNA, leads to data for a force-extension relationship.

First section will explain what the process is achieve to FEC's, proceeded by explaining what to do with FEC's.

6.1.1 Data processing

Two sources of data were used to create force-extension curves; a photo diode and a piezo stage. Explained in [Calibration using power spectrum method] the photodiode detects the scattered laser from the optically trapped bead. It correspondingly produces two sets of signals relating to the bead's two-dimensional position (x,y) on the diode in volts. The signal from the piezo stage is also positional in the form of volts.

The I/O between the detectors and the user is facilitated and managed trough a customized program software interface. A generalized information flow:

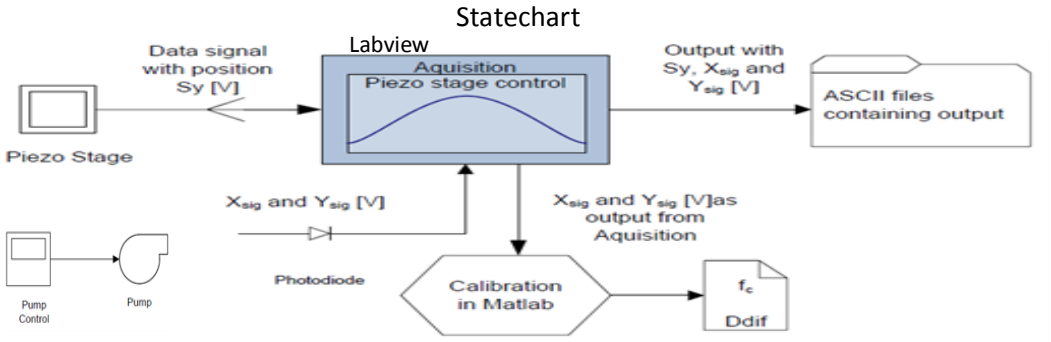

Figure 29 Acquisition, Piezo stage control, pump control developed by Ph.D. student Fabian Czerwinski.

Data is streamed into data files files and stored. The data files contain three columns of: signals y_{sig}, also being the direction of pipette displacement, x_{sig} and the stage S_y.

Igorpro, which is a data analysis software, is utilized for processing the data into force extension curves and fitting models of DNA to the data. A script compiled in Igorpro was developed for processing the data. The inputs for this script are the data file and input parameters mainly conversion factor "D_{con}" and trap stiffness k_{trap} for each of the x and y signal. The most significant output is a force versus extension dataset.

The script can be explained in a stepwise procedure.

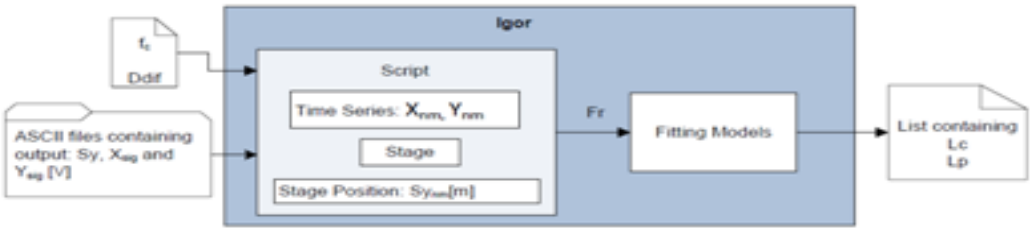

Figure 30 Script developed by Fabian Czerwinski.

At "B" in Figure 20 timeseries of the DNA grafted bead are acquired before tethering for calibrations. The input parameters k_{trap} and D_{con} are obtained by calibrating the bead. "Powerspectrum" (34) software for calibration delivers a corner frequency f_c and also a diffusion constant D_{dif} for each direction x and y. The trap's stiffness is calculated by [Calibration using power spectrum method]:

$$k_{trap} = 2\pi\gamma f_c.$$

D_{dif} can be used to calculate D_{con}. Basically $D_{dif}\left[\frac{(volts)^2}{s}\right]$ describes the diffusion of the optically trapped DNA grafted bead in the solution. D_{dif} is a fitted value based on data of a trapped beads motion [Calibration using power spectrum method]. With this constant the other input parameter, the conversion factor, can be calculated by:

$$\mathrm{D_{con}} = \sqrt{\frac{D}{D_{dif}}} = \sqrt{\frac{K_B T}{\gamma D_{dif}}} = \sqrt{\frac{K_B T}{3\pi\eta d}} \left(D_{dif}\right)^{-\frac{1}{2}}$$

where $\gamma = 3\pi\eta d$ and $D\left[\frac{m^2}{s}\right] = \frac{K_B T}{3\pi\eta d}$ [Calibration using power spectrum method].

First step is the conversion of the x_{sig} and y_{sig} column values into actual tangible positions. For converting the signal values given in volts (x_{sig}, y_{sig}) into length scale (x_{nm}, y_{nm}) requires $\mathrm{D_{con}}\left[\frac{m}{V}\right]$:

$$\mathrm{D_{con}(x)} \cdot \mathrm{x_{sig}} = x_{nm} \quad and \quad \mathrm{D_{con}(y)} \cdot \mathrm{y_{sig}} = y_{nm}.$$

Converting the mV values from the piezo stage is done in one step:

$$S_{y_{nm}} = S_y\, mV * 10000\, \frac{nm}{mV},$$

where the last constant is calibrated by the equipments manufacturer.

Figure 31 shows the measured displacements: y_{nm}, x_{nm} and Sy_{nm}, including the calculated extension of DNA: y_{DNA}. The coordinate system's center represents the center of the trap. The circles represent beads; blue: optical trapped; red: sucked to the inlet of a pipette. The green string between the circles illustrates a tethered DNA. A lighter, purposely horizontally shifted, version of the bead and pipette indicate their vertical posi-

tion before their movement. In this case the trapped bead has not been aligned with the pipette. The resulting force is also distributed along the x-axes.

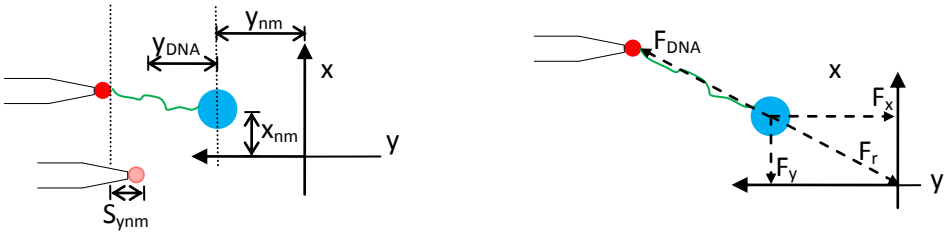

Figure 31: Schematic non-scale scenario of the force distribution and displacements while stretching a DNA molecule. y axes represent in which the pipette moves.

Next step is to calculate the force applied on the dsDNA when it is extended. When the small bead stretches the dsDNA, the molecule correspondingly pulls the trapped bead subsequently exerting a force on the trapped bead. The trapped bead is equilibrated by the optical trap, with a force equal in magnitude but in opposite direction. The force is equitable to the force on large bead by the trap:

$$F_{DNA} = F_{trap}\,.$$

Right side of the equation is known:

$$F_y = y_{nm} k_{trap_y} \;\; and \;\; F_y = y_{nm} k_{trap_y}$$

The resulting force is:

$$F_{trap} = F_r = \sqrt{F_x^2 + F_y^2}.$$

The last term compensates for the non aligned scenario in Figure 31. With the force F_r known the last step is to acquire the extension of DNA y_{DNA} for F_r vs. y_{DNA}. Displacing the pipette Sy_{nm} displaces the trapped bead y_{nm}, both are known. The simple task is to subtract them to give the extension of DNA y_{DNA}: of the:

$$y_{DNA} = \sqrt{\left(S_{y_{nm}} - y_{nm}\right)^2 + x^2}$$

The Pythagoras's theorem compensates for a deviation in alignment.

After executing the last part curves are shown.

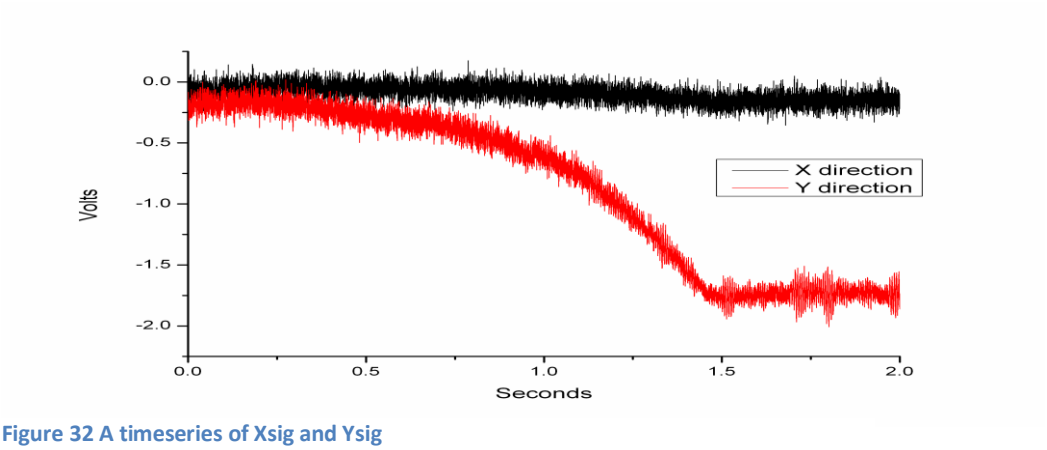

Figure 32 A timeseries of Xsig and Ysig

Figure 32 a timeseries shows data of a tether being extended. In this case the PSD has not been aligned so that the x and y signals initial mean is not around zero which is interpreted as the traps center in Figure 31. This is corrected for in the script. Oscillation is due to the beads thermal motion. This plot correlates with the stage movement Figure 33.

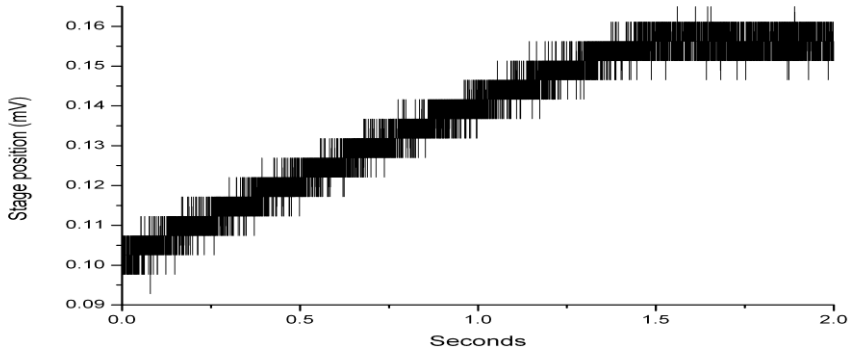

Figure 33 Stage signal Sy

Figure 32 and Figure 33 before 0.5 sec. shows that while the stage is being moved the bead does not. This must be due to the DNA being extended albeit not taut enough to exert a force to pull the bead. Figure 32 around 1 sec. shows the mean being displaced corresponding to the bead being pulled away from the trap center. Illustration Figure 31 shows that if the signal has negative values those are compensated in the calculations: e.g. due to symmetry distinction the sign of x_{nm} has no barring. In Figure 32 the x_{sig} does display a deviation from the initial mean when the bead is significantly pulled away. It shows that the pipette might not have been completely aligned.

Filtering, smoothing.

Figure 33 also shows what seems like digitized steps, which does not show on the stage controller. This has likely something to do with the electronic. The true value is the mean of the curve. Smoothing with an averaged box cart is used with a window of 400 (4). The displacement of the bead due to extension of the DNA is of interest and not the Brownian motion. To suppress the thermal motion a Savitsky – Golay smoothing filter is used on the signals with polynomial regression of 2nd degree with a window corresponding to 100Hz. This approach which leaves out a mean is not uncommon. The advantage of using this filter is its feature to retain maximum and minimum peaks, which might not de due to thermal motion.

6.2 Explaining the DNA model.

An external *force* can stretch DNA whereby it undergoes *conformational* changes leading to a change in its *entropy*. This change can be described by *elasticity* through an *energy* relationship based on *stiffness* trough *persistence length* (P) and *contour length* (Lc).

6.2.1 External force exerted on DNA: conformation change.

A simple way to explain and demonstrate the effect of entropy is by heating up a rubber band which is stretched out. The band will contract, an effect driven by entropy. As more conformations are accessible to the rubber band its entropy increases, since entropy describes the randomness of a system: $S = -k_B * \sum_i P_i \ln P_i$, P_i the probability of the system being in state "i". Same analogy can be used for DNA. At the outset DNA should be in its equilibrium state, and energy is required to deform it. In Figure 31 DNA receives thermal energy from surrounding molecules. Increased thermal energy transferred to DNA increases its internal energy which resorts to it having increased configurations at its disposal. The DNA is then in more coiled configurations with an increased entropy, a non spontaneous process.

DNA can be seen as to an entropic like spring. When stretched by an external force the entropy decreases since fewer conformations are available. As a result the spring exhibits entropic elasticity when a restoring force is generated driving the spring to it relaxed equilibrium state. When the external force is removed the entropy will increase as it will have more coiled configurations. By extending the length x of an actual spring a force is required, a relationship described by Hooke's law:$F = -K_{spring} \cdot x$. This model can be extended to materials which can be elongated and react linearly. This model cannot be applied to F-E measurements of DNA since FEC's are not linear [Figure 35: Black curve based on experimental data. Blue and green curves simulated data with

constant Lc of 1100 nm.]. K_{spring} characterizes the intra-molecular interaction of a spring the same notion can be applied to generalize DNA. Although its components work cooperatively, its mechanical properties can be simplified to parameters like P, by studying the general mechanical reaction of F-E.

6.2.2 Entropy: property of the material

Energy required to overcome the resistance to bending can be defined as (35):

$$E = \frac{k_b T Y I \theta^2}{2s}.$$

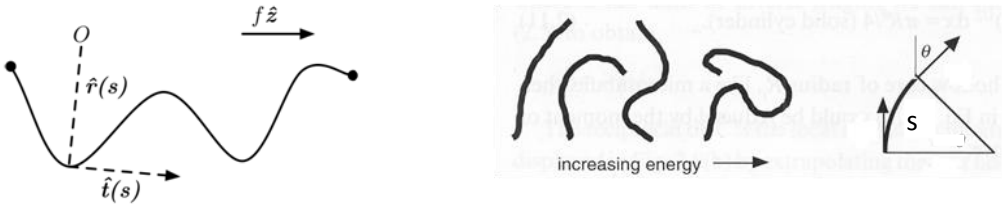

Figure 34: A homogenous molecule described by: $\hat{r}$(s) position vector as a function of the Lc where s is a point on Lc. Its unit tangent vector: $\frac{\hat{r}(s)}{ds} = \hat{t}(s)$ with respect to line segment (36)- As thermal energy increases the molecule can be in more coiled configurations (35).

Y being Young's modulus which describes the stiffness of a molecule related as [stress] =*Y**[strain] in units of Pascal. It depends on the molecule's composition. *I* is the moment of inertia of the cross section in units of length to the power of fourth. It relates to the geometry of the molecule by the size and shape of the cross section. Both are characteristic properties of the DNA and refer to its rigidity [energy]*[length]. *s* distance of a segment between two point along the contour length (L_c) of the molecule, θ the two points relative angle described as (35):

$$\langle \theta^2 \rangle \cong \frac{k_b T 2s}{YI},$$

which is valid for small angles. One way of describing the "willingness" to bend is with the persistence length (35):

$$Lp[m] = \frac{YI}{k_b T}.$$

It describes the length scale at which DNA is stiff and is a characteristic trait of DNA based on its rigidity. In Figure 34 the correlation between the two tangent vectors of two points over a segment s can be written as (35):

$$\langle \hat{t}(0) \cdot \hat{t}(s) \rangle = e^{-\frac{|s|}{Lp}}$$

The correlation function describes the physical significance of Lp. The function decays exponentially, as the segment length increases over Lc and the tangent vectors deviate in direction. Correlation is high over short segments which are relatively straight, but is

lowest for the entire molecule Lc. If length of Lp increases it leads to a low Θ where the vectors and L_c straighten out, indicating a stiffening of the molecule. If Lc > Lp then the DNA is less rigid and more convoluted.

6.3 Mathematical models of DNA: Elasticity

Two models for DNA are used in this thesis. Both theoretical models describe the force extension profile of single dsDNA, in the force regimes of the experiments where the extension never reaches Lc. Fitted values from these models are Lc and Lp. If there is a difference in Lp it implies changed features of the F-E relationship.

These two models were chosen due to a constraint in achieving forces above 25 pN, and availability of comparable data. Other models could have been used but would be redundant.

6.4 Worm like chain model.

The Kratky-Porod worm like chain (WLC) model defines the molecule as having a continuous elastic medium. The energy of the molecule can be described as follows (36):

$$\frac{E}{k_B T} = \int_0^{L_c} \left[\frac{Lp}{2} \left| \frac{d\hat{\boldsymbol{t}}(s)}{ds} \right|^2 - \frac{F}{k_B T} \hat{\boldsymbol{t}}(s) \cdot \hat{\boldsymbol{z}} \right] ds.$$

$\left(\frac{d\hat{\boldsymbol{t}}(s)}{ds}\right)^2$ is the curvature of the molecule, F being the applied force. A force-extension relationship derived from the Kratky-Porod energy formula has been obtained by accurate (35) interpolation (37):

$$\frac{FLp}{k_B T} = \frac{1}{4}\left(1 - \frac{x}{L_c}\right)^{-2} - \frac{1}{4} + \frac{x}{L_c} .$$

This model, and its derivatives, has been used extensively. The model can be used for dsDNA for forces in the entropic regime (37). DNA molecules elasticity arises from its resistance to entropy loss. Beyond that the elasticity is dominate by enthalpic contributions where the chemical bonds of DNA are modified (38). When the DNA is extended close to Lc the model increases faster than the dsDNA, due to the model being inextensible (39). Figure 34 shows experimental data with two simulated WLC models with a constant Lc of 1100 nm and Lp 15 and 30 nm. The form of the FEC becomes sharper as Lp is increased. When a molecule is extended and subsequently a change in its conformation makes it stiffer, that in turn, requires more force to keep the molecule held.

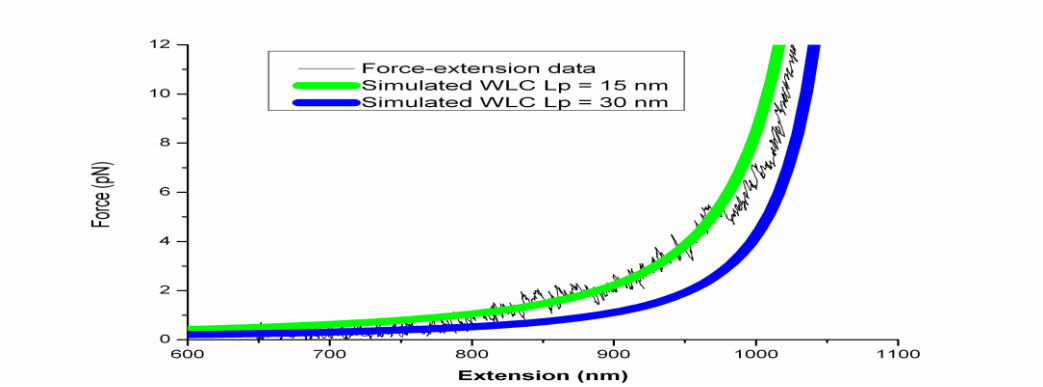

Figure 35: Black curve based on experimental data. Blue and green curves simulated data with constant Lc of 1100 nm.

Due note, the goal is not to test the validity or the robustness of the models.

6.4.1 Winkler.

The Gaussian Winkler model describes the DNA as a chain of Gaussian segments (40):

$$\frac{FL_cLp}{k_BT} = \frac{3x}{2\left(1-\frac{x^2}{L_c^2}\right)^2} .$$

The distance between each point along Lc is Gaussian distributed. The main underlying difference between the two models is that in the case of WLC the magnitude of the tangent vector **t**(s) is constrained to one unit. In the Winkler model the magnitude of **t**(s) is not one but it is constrained to an average $\langle \boldsymbol{t}(s)^2 \rangle$ (40). The model assumes that the DNA has a certain internal elasticity which this model can compensate. This intrinsic elasticity of the Winkler model results in Lc not being fixed due to the segments in the model also fluctuating; with fitted Lc values obtained being larger (41). Since there is an inherent underlying difference in the models the force extension relationships are also "different".

Both models are not completely correct as they do not consider the chemical structure of the DNA or the solvents. Nor do they assess rotational and vibration modes which contribute entropic elasticity (42). The main objective is to detect a change in FEC's and or a difference in the values of Lp.

The main point in this section was that conformation change in DNA leads to different elastic properties which can be described by Lp.

7 dsDNA & C_{60}

For all experiments laser power output was 1.6 W, stage velocity was 200 nm/s and was moved 400 nm, with an acquisition rate of 10kHz. Force-extension curves presented in this thesis have only been smoothed with an average box cart with a window of 50. This should give a sense of how the raw data looks like where minor deviations from the mean are visible.

Only those dsDNA molecules which were exposed to C_{60} during experiment were analyzed. For each extension and relaxation process their corresponding data was analyzed separately. This means that the data presented is for several dsDNA molecules where each process is treated independently.

Successful extension-relaxation related data was discarded if no extension-relaxation experiments were possible when C_{60} was flushed in.

7.1 Presentation of force extension curves

This section will present data acquired regarding extension and relaxation of single dsDNA, first without then with C_{60}. Emphasis is on one result from extension of dsDNA. Where after it will be shown that this result is not unique with multiple superimposed curves showing the same pattern. Comparing the averaged curves for extension and relaxation data will show a similarity in trend. At the end analysis with regards to Lp's through statistical tests will be presented, showing the level of significance of correlation between data if any.

7.1.1 Data for single stretching dsDNA

A single force extension relationship undergoing extension, for dsDNA in KD buffer, is illustrated in Figure 36. The horizontal axis, refers to the extension of the molecule scaled in nm, with a range of [600:1100] corresponding to data points within approximately 650-1050 nm. The vertical axis [0:12] illustrates the force exerted on the molecule in pN, from 0 pN to at least 12 pN. The blue outlined curve represents data related to experiments.

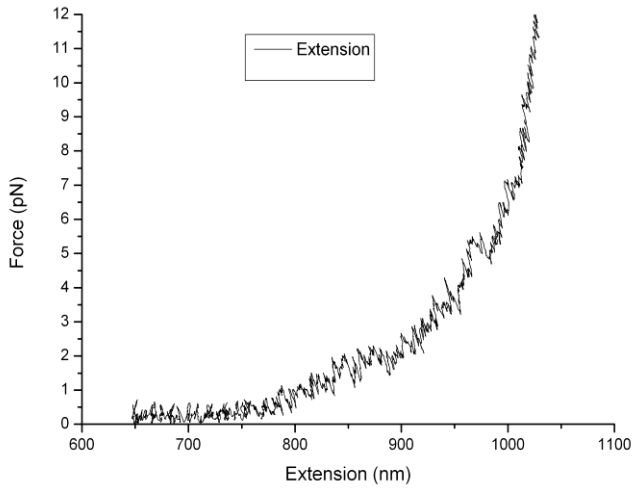

Figure 36 Graph showing a FEC of a dsDNA when undergoing extension.

Oscillations in the trace are prevalent throughout the length of the curve. Higher force fluctuations in the form of peaks deviating from the mean are also present in the vertical scale. Notwithstanding the oscillations and fluctuations, a segment of the extension ranging from the initial extension about 650nm up to 750 nm, displays a 'constant' force plateau with near zero gradient. In this regime the force is below 1 pN. An increase in force is observed of above 12 pN, as extension approaches Lc from 900 nm. The force-extension ratio increases albeit with a non-linear inclination.

A representative presentation of force extension data was illustrated in Figure 36 and described. To show the tendency and trend of the F-E experiments, graphs for three extension procedures were merged and displaced for visual comparison in Figure 37. The axis is scaled and defined as in Figure 1.

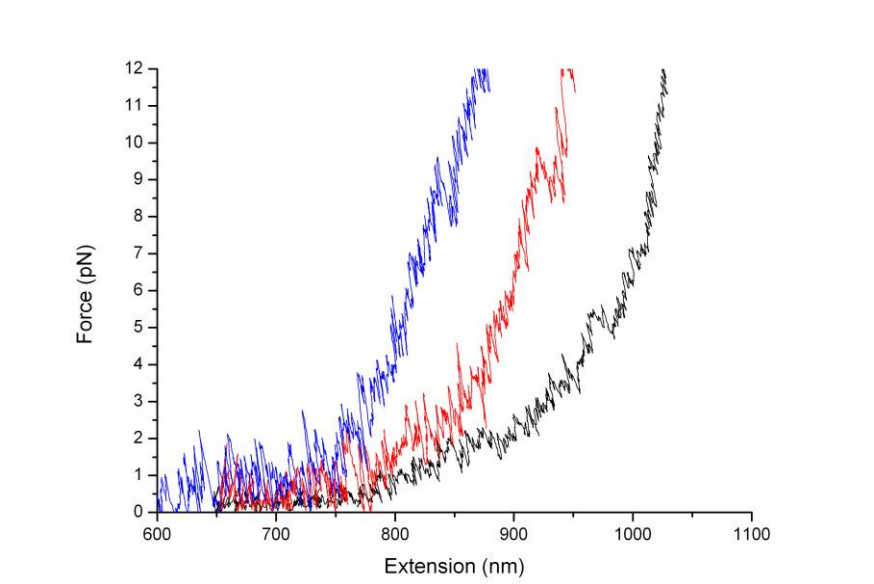

Figure 37 Three force-extension curves when extending a dsDNA. The blue and red have been displaced to the left.

Their overall form and trend are the same as described with respect to Figure 36. They show same characteristics and features: a segment with barely zero gradient constant force, another segment with an inclination. Albeit overall alignment, discrepancies persist with oscillations and peaks, but notably the curves do not exactly overlap.

7.1.2 Relaxation data

Note the pink outlined curve plotted in Figure 38 which is data from the relaxation of a dsDNA molecule illustrating the force extension relationship. Again the horizontal axis is the extension of the DNA in nm versus the force subjected to it in pN. Both axis are scaled comparable to the previous figures.

For the relaxation data multiple curves were transposed into a single graph not shown. They illustrated that the blue curve in Figure 38 is not unique due to them being superimposed very well on each other showing the same repeated forms and characters.

7.1.3 Comparing extension and relaxation curves

A comparison between the relaxation and extension curve is shown in Figure 38. The blue and pink outlined curves are data for extension of dsDNA, black and green the extension. They show a resemblance in form and features as they show same trend.

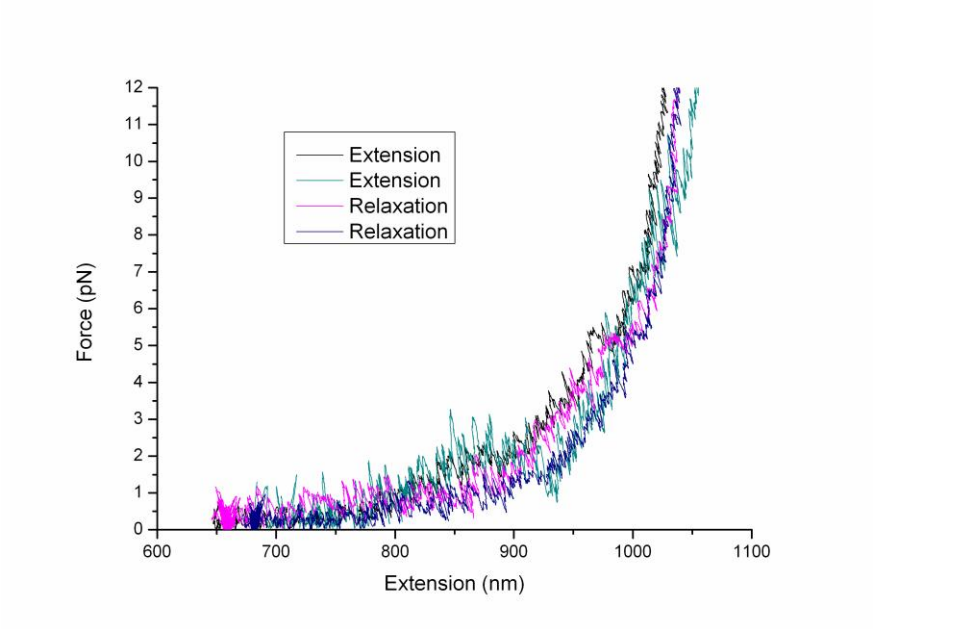

Figure 38 Two extension curves and two relaxation curves are plotted.

Additional data has been added to the pink outlined curve for data relaxation located at approximately 650-680 nm. An increase in accumulated data points is visible at that interval, corresponding to where the pipette was held stationary before the piezo movement.

The quest was to present some representative data visually and point out the main observed highlights of the force extension relationships. It has been deemed sufficient to visually confirm the characteristic differences and correlations of the curves. The main point to infer is that the mechanical process to extend and relax a dsDNA molecule is in this case the same. Although each curve is not exactly the same they are comparable. Comments and elaboration follows in [Discussion: bare dsDNA].

7.2 Analysis

The analysis of FEC's involves fitted values for Lc and Lp. Statistical tests on both types of values will be employed to gauge if there is any correlation or difference between the values. Results are discussed in the next section.

All the FEC's were fitted with the WLC and Winkler models in the range from 10 pN down to the base line below 1 pN. Each fit returned two parameters Lc and Lp.

Table 1 contains the mean and standard error (SE) values for Lp in units of nm from measurements of extension and relaxation, fitted for both models. These are for values before the introduction of C_{60}.

Table 1: Fitted values for Lp in nm (mean ± SE; n = 6), n is number of experiments, in the absence of C_{60}.

Model	Extension	Relaxation
WLC	11.3 ± 0.9	12.5 ± 1.6
Winkler	17.5 ± 3.0	16.3 ± 2.0

The differences between extension and relaxation values within their corresponding models seem negligible considering their SE. Both the mean and SE are higher from Winkler model than the WLC model.

Probability tests were performed to investigate if there were any significant differences between the means in Table 1. Student's t-test was used with the assumption that the datasets have equal variance. The results for different combinations are given in Table 2.

Table 2: Statistical tests for results without C_{60}. Student's t-test, with equal variance.

	p-value
WLC: Extension vs. Relaxation	0.526
Winker: Extension vs. Relaxation	0.737
Extension: WLC vs. Winkler	0.072
Relaxation: WLC vs. Winkler	0.177

Throughout the combinations tested there is a significant correlation in them. Strongest correlation is within the models. Highest probability of the means being different is when the models are compared.

Values associated with experiments performed in C_{60} are depicted in Table 3 with mean and SE of Lp values in nm.

Table 3 Fitted values for Lp in nm (mean ± SE; n = 5), n is number of experiments, in the presence of C_{60}.

	Extension	Relaxation
WLC	33.4 ± 4.4	39.1 ± 3.4
Winkler	47.5 ± 6.5	56.9 ± 5.5

All values are higher than those in Table 1, including their SE. Values from the Winkler model are again higher.

Again Student's t-test was used to find if there was any significant difference between the means of Table 3. The probability values from the tests are given in Table 4.

Table 4 Statistical tests for result with C_{60}. Student's t-test, with equal variance.

	p-value
WLC: Extension vs. Relaxation	0.337
Winker: Extension vs. Relaxation	0.336
Extension: WLC vs. Winkler	0.109
Relaxation: WLC vs. Winkler	0.029

There is a significant difference between the means of extension data from WLC and Winkler. There is a higher probability of no difference in the means within the models. This concurs with values in Table 2.

Final set of t-tests were to compare results for in presence and absence of C_{60}. The combinations are given in Table 5 with corresponding probability values.

Table 5 Statistical tests for result with C_{60} and without C_{60}. Student's t-test, with equal variance.

C_{60}: With vs. Without	p-value
WLC: Extension	0.00046
WLC: Relaxation	0.00004
Winkler: Extension	0.0015
Winkler: Relaxation	0.00004

It can be concluded that there is a very significant difference between their respective means.

Descriptive statistics can be utilized to observe a pattern in the data's distribution and to compare different distributions. A box plot visually illustrates if the data is skewed and it is easier to detect points which deviate. The box is plotted according to data distributed in percentage tile from the least to the highest value. The whole box contains middle 50 % of the data, where the upper edge defines 75 % and the lower edge 25 %. The line through the box indicates the median of the data; top 50 % of them are above it, and top 25 % above the box. The ends of the two beams extending out of the box represent one standard deviation above and below the mean. Points further away are defined outliers. The small square is the mean. Data points are illustrated as dots. The horizontal axis is only used to create a distance. The curves are the normal distribution of the data.

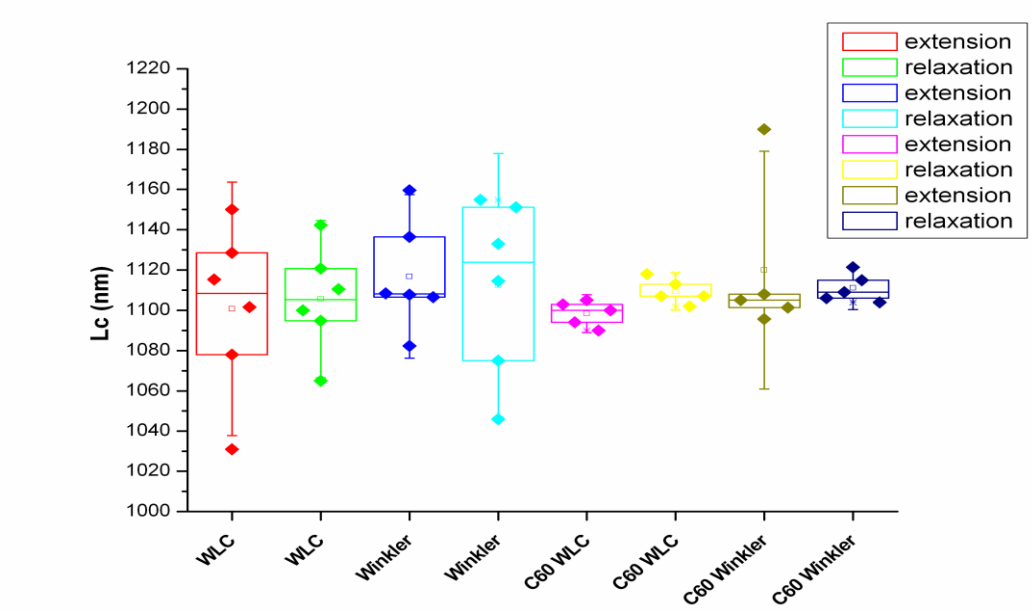

Figure 39 Box plots of Lc from all experiments. Plot includes data from both models.

Figure 39 shows box plots of Lc's for all experiment and for both model. 1100 nm is the theoretic value. There are only two outliners. Data from C_{60} experiments are spread least. "Winkler-extension" seems to be the most skewed box, tilting towards Lc. Nonetheless all the boxes can be seen close to Lc. For Lc's without C_{60} the boxes indicate slightly higher values for Winkler models.

8 Discussion: bare dsDNA

This section is divided up into two subsections, one shedding light on the force extension curves and the other highlighting Lp values.

8.1 Mechanical characteristics from curve form

The achieved pattern of FEC's is what was expected and corroborate with previously performed experimental results (41) (37). The patterns of multiple FEC's in Figure 37 also verifies same similarities in trend of force extension scaling. The FEC's superimposed in Figure 38 should have overlapped suggesting the same mechanical behavior description for extension is applicable for relaxation.

Elaboration of the FEC Figure 36 follows.

From the initial extension up to about 1050 nm and to less than 10 pN, the DNA's extension is less than its Lc, as it begins to straighten out. What is observed is a decrease in entropy coupled to an increase in force. Even before extending the DNA it is te-

thered, this removes conformations leading to lower entropy. This implies that there is a force on the DNA even when it is initially stationary. Relative small contractile forces are present up to approximately 1050 nm due to dominant entropic elasticity. Increased extension precludes more conformations and results in higher entropic forces. The work done is against entropic forces with the extension nearing Lc, as DNA drives toward more conformations (43) (35) (44) (39). Bending of DNA due to thermal energy is reduced.

What is observed from around 10 pN and 1050 nm is the beginning of a sharp linear force response to stretching (43) (37) (38). The B-form DNA is almost stretched "tight" as the backbone starts to deform by lengthening of Lc (43). The increased stiffness and intrinsic elastic behavior is enthalpic where chemical bonds are slightly modified (38). Close to Lc enthalpic forces become important, where also the bends on DNA cease to exist, due to its reduced entropy (43). Due to the restriction on the forces which could be applied, the enthalpic contribution could not be investigated.

Figure 37 should have depicted cycles of extension and subsequent relaxation of dsDNA. All of the curves should have been aligned. The area between the curves is the work done by the spring. It seems work is done since either pathways do not overlap completely: $H = \Delta S = F \Delta X \neq 0$ i.e. they do not exhibit same entropic. The entire process is arguable not in equilibrium and reversibility of the mechanical process of extension and relaxation does exhibit mechanical hysteresis, but is there a change in the DNA's bond configurations? If there is how would that have happened, since nothing is introduced into the fluidic system but the buffer?

8.2 Persistence length and contour length

Data for Lc's have been depicted in Figure 39 from all experiments and both models. Their spread has been shown in plot boxes. Only four points from the Winkler model are below Lc whereas 10 values from the WLC model are at or below Lc. This might be due to the fact that the tangent vector used to describe the DNA model is an average and not fixed to unit length of 1 like in the WLC model (35) (40). Due to this there should be a difference as can be observed in Figure 39 and which concurs with (41). If a 5 % margin is acceptable around Lc only 2 points fall outside it is possible to infer that the sets of data are comparable and fairly centered around Lc. Which would mean that the models to fit well to Lc.

Table 1 lists means with SE of Lp from WLC and Winkler model measured on dsDNA molecules. Their means are not far apart considering their SE. There is a difference in Lp values with those from the Winkler model being higher than those from WLC model as

concurs with (41). Table 2 explains that values for extension and relaxation do correlate for each model.

The mean of the measured Lp's seem rather low compared to what is referenced in the literature 52 nm (35). The difference being nearly 40 nm or about 4 times higher seems significantly large. Lp is intrinsic to the DNA [Entropy: property of the material]. A change in the configuration in the molecule would correlate to a difference in Lp [Entropy: property of the material]. The experiments were performed in a solution of relatively high ionic strength 100 mM NaCl and 20 mM MgCl. Since the DNA has a negatively charged backbone of phosphate groups a relative high concentration of Mg^{2+} and Na^{+} ions would reduce the electrostatic repulsion between (35) (37) (44). Decreasing the energy required for deformational change leads to increase flexibility where the DNA is more coiled up which intuitively means the stiffness of DNA Lp has decreased. Lp depends on ionic strength (44) (37), and the differences in Lp are therefore probably due to different conditions of solutions. In this case a shorter Lp indicates that the molecule is more flexible, and relatively more condensed and e.g. less likely to extend further from the bead surface before tethering.

In (41) dsDNA F-E experiments were performed and the results fitted with WLC and Winkler models. The fits were restricted up to 10 pN.

Buffer	WLC (nm)	Winkler (nm)
137 mM NaCl	16± 5	21± 4

Theoretical values are larger than values from Winkler are larger than those obtained from WLC. Their values were found to be consistent with (37). These values are higher although within range of Table 1. Notice the higher ionic concentration which most likely attributed the higher values. Considering the ionic concentrations the values from (41) are comparable to those in Table 1.

9 Result of adding C_{60} buffer

In this section data for experiments with C_{60} will be presented. It is possible to detect changes in conformation of DNA through FEC's, by using appropriate models from which Lp's are obtained. That is discrepancies being those between experimental data with (bare-data) and without C_{60} (C_{60}-data).

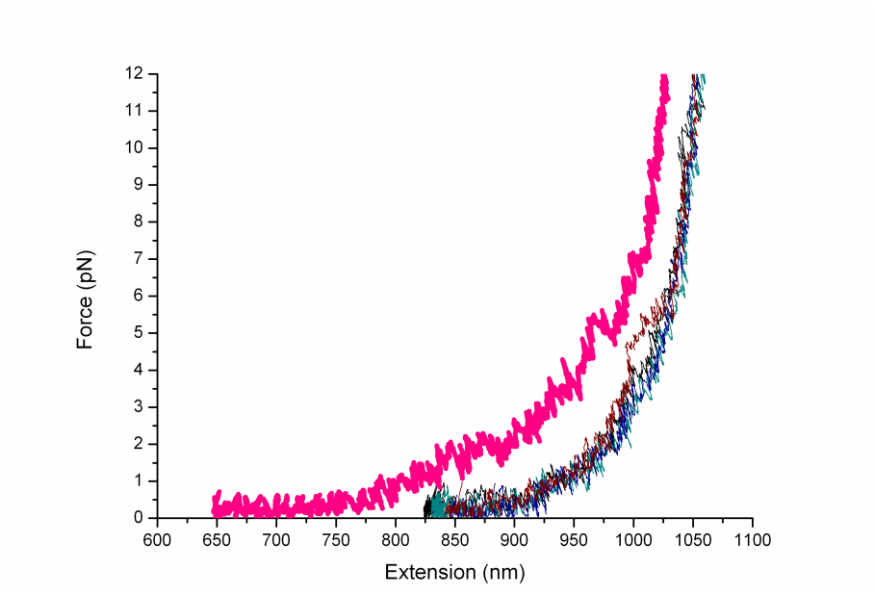

Figure 40 Thick pink FEC without C_{60}, 6 other with C_{60} half of them relaxation.

Graph **Error! Reference source not found.** depicts multiple FEC's, one thick pink outlined without and the rest with C_{60}. The main observed differences are as follows:

At the baseline, where the force is around 1 pN, there is a difference between the two curves. In that the base segment is shorter for C_{60}-data than of bare-data. In the case of C_{60}-data the initial extension of the DNA has relatively increased. This suggests that the DNA has been condensed or shortened before it was extended.

Another significant difference is the force, which increases at a faster rate for C_{60}-data than for bare-data. The increased inclination occurs near the foot of the baseline up to around 9-10 pN, where after the inclination seems the same. For C_{60}-data the gradient of this part of the curve although steeper is over a short segment. Whereas bare-data exhibits a gradient change more gradual over a longer segment.. The other point would be that effectively less work is required to reach the enthalpic regime, since work has already been done on the DNA by reducing the DNA extension.

The entropic forces increase as conformations are decreased. This suggests that since the entropic forces have increased, by extending the dsDNA-with C_{60} over e.g. 200 nm compared to bare-dsDNA, a decrease in conformation might have followed. Change in force-extension in this region might reflect entropic change in DNA.

The multiple FEC's do overlap much more than those in Figure 38. It is doubtful that the difference in relaxation and extension observed in Figure 38 is due to some mechanical malfunction e.g. objective pulling the bead down through the x and y plane, since that would also manifest itself in Figure 40. Does the C_{60} apart from stiffening the dsDNA make it somehow "stable"; in the sense that all dsDNA exposed to C_{60} will exhibit more of the same F-E relationship?

Nonetheless, when C_{60} is present it does change the dsDNA's elastic entropic response, which suggests a change in dsDNA's configuration when exposed to C_{60}.

9.1 Discussion of adding C_{60} buffer

Since there is a difference between force extension relationship with and without the addition of C_{60}, this must mean that the conformation of dsDNA has changed. A conformational change should be reflected in its Lp value. A higher rate of increase in the force extension curve suggests a stiffer molecule. Table 3 lists the mean and SD for Lp which are higher than those in Table 1. This implies that dsDNA in the presence of buffer with C_{60} is more stiff. Comparing their means through t-test shown in Table 5 gave probability values below 0.01 signifying a substantial difference.

The t-tests together with actual difference in the force-extension curves, it is possible to infer that dsDNA has a different conformation in the presence of C_{60}.

FEC's of C_{60}-data have been displaced shows the general trend for both extension and relaxation. They also show both mechanical processes aligned and overlap, indicating that no work is generated out of the cycle. T-test for extension and relaxation for each model in Table 4 infers that there is not a significant difference in relaxation and extension.

As explained in [Dissolving C60] nC_{60} might form a complex where around it the pH is basic. There is also a possibility that is can form ionic bonds with Mg^{2+} and Na^{1+} in the solution. This opens up the possibility of nC_{60} interacting with the backbone of dsDNA either by ions reducing the electronegative repulsion. Also explained was that nC_{60} has a negative charged outer shell [Dissolving C60]. On the other hand laboratory experiments related to this work showed unspecific binding of nC_{60} to pipettes, dsDNA grafted bead and anti-DIG beads. Even with a negative charged shell nC_{60} there is a possibility that it can adhere to dsDNA.

10 Conclusion

The goal of the main project was to investigate if C_{60} interacts with dsDNA, by using optical tweezers to probe the elastic response of a single dsDNA molecule, before and after the addition of C_{60}.

The C_{60} molecule's indirect contribution as a toxic promoting agent has been studied.

It was possible to carry out force-extension measurements by extending and then relaxing dsDNA, whereby an elastic relationship was profiled using theoretical models, the Winkler model and the WLC model from which persistence lengths were obtained which describes DNA's flexibility. A buffer with C_{60} would be flushed into microfluidic by a precision pump and a repetition of the force-extension would be measured.

Result obtained in the main project shows:

The force-extension curves showed a general tendency of initial low force with an increase when the extension neared the contour length. Curves showed a difference in response when C_{60} is present. An increase in rate of force in response to extension of DNA, and an increase in the initial extension is also shown.

In the absence of C_{60} persistence lengths were relative short: WLC extension: 11.3 ± 0.9 nm, relaxation: 12.5 ± 1.6 nm; Winkler extension: 17.5 ± 3.0 nm, extension: 16.3 ± 2.0 nm implying the dsDNA being flexible and more coiled. T-test were performed which showed no significant difference between extension relaxing WLC 0.526 Winkler 0.737.

Persistence length were longer when C_{60} was present, indicating a stiffening if the molecule WLC 33.4 ± 4.4 nm 39.1 ± 3.4 nm Winkler 47.5 ± 1.6 nm6.5 56.9 ± 5.5 nm. T-tests also showed a significant difference in the presence and absence of C_{60} with the highest p-value 0.0015.

C_{60} forms aggregates which adhere to dsDNA grafted bead, anti-Dig coated beads and the glass pipettes. It might be due to the aggregates of C_{60} which attach to the dsDNA, either unspecific adhere like observed or the ions of the solution reduce C_{60} electronegative density decrease the repulsion between them. By this the DNA should become stiffer by locking parts of the DNA.

The toxic affect of C_{60} by altering or damaging dsDNA is supported by the results of this thesis (physical change).

Investigating the toxic affect of C_{60} becomes more relevant as the spread of such material increases both in quantity but also into different industrial sectors including

health and beauty. The daily amount of exposure to such material is thus rapidly increasing. Physical attached blocking translation of DNA and enzymes and repair.

Furthermore, the goal of one of the side projects was to improve the trapping efficiency of the laser trap quickly and in an inexpensive manner. This was done by changing the collar correction value of the water objective with varying cover glass thickness with a trapped bead, since the objective is not optimized to be used with a laser.

Results associated with this project showed a maximum achievable trapping stiffness for each cover glass thickness with a corresponding specific collar value. The result was used in the main project

Another subproject's objective was to study the flow profile of the custom built fluidic chambers used in the main project by trapping and calibrating a bead throughout the height chamber, when applying a constant flow by a pump. The pump was also used in the main project.

The result showed that a drag force is measurable on the bead and highest at the center of the chamber and lowest the edge of the chamber following a parabolic profile. It was possible to conclude that the fluidic chamber in conjunction with the pump created a constant velocity flow profile which follows that of a parabolic as what the related theory suggests.

10.1.1 Future work

In the future there could be an optimization in the method for achieving results. This could be done by improving the dsDNA handles to extend beyond the entropic regime and thus investigate the force plateau, enthalpic regime and hysteresis. If one introduces C_{60} while having the dsDNA extended, whereby measurements of contraction of dsDNA. It might be prudent to increase the salt concentration to achieve higher persistence length, since those achieved seem small. Another material which is easier to dissolve and one or two parameters can be changed to see its effect on dsDNA.

11 Bibliography

1. *Stable Colloidal Dispersions of C Fullerenes in Water: Evidence for Genotoxicity.* **Dhawan, ALok, et al.** 23, s.l. : Enviromental Science & Technology, 2006, Enviromental Science & Technology, Vol. 40, pp. 7394-7401.

2. *Oxidatively Damaged DNA in Rats Exposed by Oral Gavage to C60 Fullerenes and Single-Walled Carbon Nanotubes.* **Folkmann, Janne K., et al.** 5, s.l. : Environmental Health Perspectives, 2009, Environmental Health Perspectives, Vol. 117.

3. **Ashkin, Arthur.** *Optical trapping and manipulation of neutral particles using lasers.* s.l. : Biophysics, 1996. pp. 4853-4860.

4. **Trpcevski, Dejan.** *Optical Stretching of DNA as a Diagnostic Tool in Nanotoxicology.* Niels Bohr Institute, University of Copenhagen. 2006. Cand. Scient. thesis.

5. **Tolic´-Nørrelykke, Simon Flyvbjerg.** *A single molecule study of RNA polymerase and TATA-box binding protein.* Niels Bohr Institute, University of Copenhagen. 2002. Ph.D. thesis.

6. **Lentge, Heidi.** *Kontruktion og afprøvning af en optisk pincet.* Niels Bohr Institute, University of Copenhagen. 2005. Cand. Scient. thesis.

7. **Ukita, Hiroo and Saitoh, Takashi, Sakahra Noboru.** Resolving Discrepancy between Theoretical and Experimental Optical Trapping Forces Using Effects of Beam Waist and Trapping Position Displacement due to Gravity. *Optical Review.* september 7, 2006, Vol. 13, 6, pp. 436-442.

8. **Griffiths, David J.** *Introduction to electrodynamics.* 3. edition. s.l. : Prentice Hall, 1999.

9. **Mazo, Robert M.** *Brownian Motion Fluctions, Dynamics and Applications.* Oxford : Oxford Science Publications, 2002.

10. **Odderhede, Lene, et al.** Optical Tweezers: Probing Biological Surfaces. *Probe Microscopy.* 2001, pp. 129-137.

11. **Brody, James P., et al.** Biotechnology at low reynolds numbers. *Biophysical Journal.* 71, December 1996, pp. 3430-3441.

12. **Berg, Howard C.** *Random Walk in Biology.* Expanded edition. Chichester : Princeton University Press, 1993.

13. **Roger, Bowley and Mariana, Sánchez.** *Introductory Statistical Mechanics.* 2nd. s.l. : Oxford Science Publications, 1999.

14. **Hecht, E.** *OPTICS.* 4 ed. San Fransisco : Addison Wesley, 2002.

15. **Keller, H. Ernst, et al.** Olympus Microscopy Resource Center. *Spherical Aberration.* [Online] [Cited: January 3, 2010.] http://www.olympusmicro.com/primer/java/aberrations/spherical/index.html.

16. **Abramowitz, Mortimer, Spring, Kenneth R. and Davidson, Michael W.** Common Optical Defects in Lens Systems (Aberrations). *Olympus Microscopy Resource Center.* [Online] [Cited: January 3, 2010.] http://www.olympusmicro.com/primer/lightandcolor/opticalaberrations.html.

17. **Abramowitz, Mortimer, Flynn, Brian O. and Davidson, Michael W.** Optical Aberrations. *Introduction to Optical Microscopy, Digital Imaging, and Photomicrography, 2007.* [Online] [Cited: January 3, 2010.] http://www.olympusmicro.com/primer/java/aberrations/slipcorrection/index.html.

18. **Spring, Kenneth R., Parry-Hill, Matthew J. and Davidson, Michael W.** Airy Patterns and the Rayleigh Criterion. *Olympus Microscopy Resource Center.* [Online] [Cited: January 3, 2010.] http://www.olympusmicro.com/primer/java/imageformation/rayleighdisks/index.html.

19. Numerical Aperture and Resolution. *Olympus Microscopy Resource Center.* [Online] [Cited: January 3, 2010.] http://www.olympusmicro.com/primer/anatomy/numaperture.html.

20. *A general method for manipulating DNA sequences.* **Fuller, N. Derek, et al.** February 1, 2006, Nucleic Acids Research, Vol. 34.

21. **Kroto, Harold W.** symmetry, space, stars and C60. *Nobel Lecture.* December 7 1996.

22. **Maxell, Andrew J.** electronic and Geometric Structure Studie of C60 as an Adsorbate, Solid, and Model for Graphite. *Comprehensive Summaries of Uppsala Dissertations from the Faculty of Science and Technology 223.* Uppsala, Sweden : ACTA Universitatis Upsaliensis, 1996.

23. *Spherical Aromaticity of Fullerenes.* **Buhl, Michael and Hirsch, Andreas.** s.l. : Chem. Rev., 2001, Chem. Rev., Vol. 101, pp. 1153-1183.

24. *Spherical Aromaticity: Recent Work on Fullerenes, Polyhedral Boranes, and.* **Chen, Zhongfang and King, Bruce.** 105, s.l. : Chem. Rev., 2005, Chem. Rev., pp. 3613-3642.

25. [Online] [Cited: January 3, 2010.] http://www.ch.ic.ac.uk/motm/c60.html.

26. *Formation of Aqueous suspensions of Fullernes.* **Ma, Xin and Bouchard, Dermont.** s.l. : Enviromental Science & Technology, 2009, Enviromental Science & Technology, Vol. 43, pp. 330-336.

27. *C Colloid Formation in Aqueous Systems: Effects of Preparation Method on Size, and Surface Charge.* **Duncan, Laura K., Jinschek, Joerg R. and Vikesland, Peter J.** 42, s.l. : Enviromental Science & Technology, 2008, Enviromental Science & Technology, pp. 173-178.

28. *C in Water: Nanocrystal Formation and Microbial Response.* **Fortner, J. D., et al.** 39, s.l. : Enviromental Science & technology, 2005, pp. 4307-4316.

29. *Stable Dispersions of Fullerenes, C60 and C70 in Water. Preparation and Characterization.* **Deguchi, Shigeru, Alargova, Rossitza and Tsujii, Kaoru.** 17, s.l. : Langmuir, 2001, Langmuir, pp. 6013-6017.

30. **Chaplin, Martin.** Fullerene Hydration. *Water structure and science.* [Online] [Cited: January 3, 2010.] http://www1.lsbu.ac.uk/water/buckmin.html.

31. *Comparative analysis of two aqueous-colloidal solutions of C60.* **Andrievsky, G.V., et al.** s.l. : Chemical Physics Letters, September 23, 2002, Chemical Physics Letters, Vol. 364, pp. 8–17.

32. *Studies of aqueous colloidal solutions of fullerene C by electron 60.* **Andrievsky, G.V., et al.** s.l. : Chemical Physics Letters, 1999, Chemical Physics Letters, Vol. 300, pp. 392–396.

33. *Structure of C60 fullerene in water: spectroscopic data.* **Scharff, P., et al.** s.l. : Carbon, 2004, Carbon, Vol. 42, pp. 1203–1206.

34. **Hansen, Poul Martin, et al.** Tweezercalib 2.0: Faster version of a MatLab package for precision calibration of optical tweezers. *Computer Phys. Comm.* 174, 2006, pp. 518-520.

35. **Boal, David.** *Mechanics of the Cell.* s.l. : Chambridge University Press, 2006. 0-521-79681-4.

36. **Brown, Andre and Johnson, Philip.** Wormlike chains. *Biocurious.* [Online] [Cited: January 3, 2010.] http://biocurious.com/2006/07/04/wormlike-chains.

37. *Stretching DNA with Optical Tweezers.* **Wang, M. D., et al.** s.l. : Biophysical Journal, March 1997, Biophysical Journal, Vol. 72, pp. 1335-1346.

38. *Estimating the Persistence Length of a Worm-Like Chain Molecule from.* **Bouchiat, C., et al.** s.l. : Biophysical Journal, January 1999, Biophysical Journal, Vol. 76, pp. 409–413.

39. *overstretching B-DNA: The Elastic Response of Individual Double-Stranded and Single-Stranded DNA Molecules.* **Smith, Steven B., Cui, Yujia and Bustamante, Carlos.** s.l. : American Association for the Advancement of Science, Feb. 9, 1996, Science, Vol. 271, pp. 795-799.

40. *Deformation of semiflexible chains.* **Winkler, Roland G.** 6, s.l. : JOURNAL OF CHEMICAL PHYSICS, FEBRUARY 8, 2003, JOURNAL OF CHEMICAL PHYSICS, Vol. 118.

41. *The elastic properties of single.* **Salomo, M., et al.** s.l. : Colloid Polym Sci, (2006, Colloid Polym Sci, Vol. 284, pp. 1325–1331.

42. **Niemeyer, Christof M. and Mirkin, Chad A.** *Nanobiotechnology Concepts, Applications and Perspectives.* 1. s.l. : Wiley-VCH, 2004. 3-527-30658-7.

43. *Twist and shout (and pull): Molecular chiropractors undo DNA.* **Marko, John F.** October 1997, Proc. Natl. Acad. Sci., Vol. 94, pp. 11770–11772.

44. *Ionic effects on the elasticity of single DNA molecules.* **BAUMANN, CHRISTOPH G., et al.** s.l. : Proc. Natl. Acad. Sci., June 1997, Proc. Natl. Acad. Sci., Vol. 94, pp. 6185–6190.

45. **Tolic-Nørrelykke, I.M., Berg-Sørensen, K. and Flyvbjerg, H.** MatLab program for precision calibration of optical tweezers. *Computer Phys. Comm.* 159, 2004, pp. 225-240.

46. Wikipedia. [Online] http://en.wikipedia.org/wiki/Continuity_equation.

47. Molecular Expressions:. *Introduction to Optical Microscopy, Digital Imaging, and Photomicrography.* [Online] [Cited: January 1, 2010.] http://microscopy.fsu.edu/primer/images/aberrations/spherical1.jpg.

48. **Apparatus, Harvard.** Harvard Apparatus. *Harvard Apparatus.* [Online] [Cited: August 20, 2009.]

http://www.harvardapparatus.com/wcsstore/ConsumerDirect/images/site/hai/techdocs/Pump%20Selection%20Guide.pdf..

49. **Abramowitz, Mortimer and Davidson, Michael W.** Numerical Aperture and Resolution. *Olympus Microscopy Resource Center.* [Online] [Cited: January 3, 2010.] http://www.olympusmicro.com/primer/anatomy/numaperture.html.

50. studentsguide.in. *studentsguide.in.* [Online] [Cited: February 10, 2010.] http://www.studentsguide.in/genetics/nucleic-acids/waston-and-crick-model-of-dna-structure-of-dna.html.

51. *Crystal structure analysis of a complete turn of B-DNA.* **Wing R, Drew H, et al.** s.l. : Nature, Oct. 23, 1980, Nature, Vol. 287, pp. 755 - 758.

52. DNA's B Form, A Form and Z Form. *DNA's B Form, A Form and Z Form.* [Online] [Cited: February 17, 2010.] http://www.web-books.com/MoBio/Free/Ch3B3.htm.

53. **Brown, Andre and Johnson, Philip.** Labeling lambda DNA. *Biocurious.* [Online] [Cited: December 12, 2009.] http://biocurious.com/2006/01/14/labeling-l-dna.

54. *Rh-Catalyzed Arylation and Alkenylation of C60 Using Organoboron Compunds.* **Nambo, Masakazu, Noyori, Ryoji and Itami, Kenichiro.** s.l. : JACS communications, June 13, 2007, JACS communications.

12 Appendix.

12.1 Appendix A

For the aqueous solution used in the flow chambers Re is:

$$\frac{\overbrace{1\cdot 10^{3}\frac{kg}{m^{3}}}^{\rho}\cdot\overbrace{20\cdot 10^{-6}\frac{m^{3}}{s}}^{flow\ rate}\cdot\overbrace{5\cdot 10^{-3}m\cdot 120\cdot 10^{-6}m}^{cross\ section\ of\ chamber}\cdot\overbrace{120\cdot 10^{-6}m}^{L}}{\underbrace{1\cdot 10^{-3}\frac{kg}{m\cdot s^{2}}s}_{\eta}}\approx 10^{-5}$$

With beads (4) : Referring to thermodynamics, equating the kinetic average energy at thermal equilibrium in 3-dimensions the mean velocity gives: $\frac{1}{2}m\langle v^2\rangle=\frac{3}{2}k_BT\rightarrow\sqrt{\langle v^2\rangle}=\sqrt{\left(\frac{3k_BT}{m}\right)}$. Inserting following values:$k_B\approx 1.38\cdot 10^{-23}\frac{J}{K}$, $T=300K$, $m_{bead}=1\cdot 10^{-12}g$, $\rho_{bead}=1\cdot 10^{-3}\frac{kg}{m^3}$ and by any means the lengths scale is in micro-meters. Re is well below 1.

12.2 Appendix B

Glass pipette.

We pulled our own pipettes. Tips of the pipettes are about one micron meter in diameter. Glass capillaries are sent through a cobber loop and is fastened on the top, and the bottom part is held to weight. The amount of heat the wire generates is set, so as to correspond to, the required tip size.

12.3 Appendix B.

Colloid solutions

12.3.1 Beads coated with AntiDigoxigen.

Commercially available 2.1 µm in diameter polystyrene beads coated with Anti-Digoxigenin.

12.3.2 Beads incubated with DNA.

Streptavidin coated beads with a diameter of 3.09 µm

DNA was received from Fabian Czerwinski.

Concentration of DNA 0,70 ng / µL marked as “1/100”.

- 7 µL PBS
- 2 µL bead solution
- 1 µL DNA solution

- Slow vortex for 45 min.
- 1.5 mL KD buffer

The correct concentration of ration between DNA on beads was found trough extensive trial and error. Effectively the goal is to achieve a single DNA molecule tether, and as such too small concentration of DNA would result in no tether at all. Too high concentration would, by estimates, result in multiple DNA tether, such a manner time consuming to detach the beads usually ending in a futile effort. In this case the tethered beads would close to each other, not displaying any visual Brownian motion or in some cases very little.

12.4 Appendix C

Buffer solutions used.

KD buffer.

Chemicals were taken directly from their stock solutions by use of sterile pipettes. The chemicals were kept in fridges. For regular use KD buffer was transferred to small containers with a volume of 50 mL. The buffer in 50 mL containers were filtered through a 100 nm pore size syringe filter before use.

Chemical compound	**Raison D'être**	**Stock concentration**	**Concentration**	**Amount**
Tris-HCl		1 M	10 mM	5 mL
$MgCl_2$		1 M	10 mM	5 mL
NaCl		1 M	100 mM	50 mL
MilliQ				440 mL
				Total 500 mL

49 mL of KD buffer was transferred to the 50 mL containers. 1 mL BSA of concentration 200 µg/mL was added to this solution. Bovineis is used as a pacifier for anti-Digoxigen receptor molecules. Measured pH 7.8.

MilliQ, or Millipore water is de-ionized water tapped from a machine.

12.5 Appendix D.

Solution with C_{60}

C_{60} material is in the form of a powdered substance. 9 mg of the material was put into a plastic vial. 5 mL KD buffer was added. It was sonicated for 3 hours and vortexed. This was the “stock” concentration. Lowest measureable concentration was used.